RWTH AACHEN UNIVERSITY
INSTITUTE OF AEROSPACE SYSTEMS

EcoAir (Efficient Cost Optimized Aircraft for Innovative Regional travel): A Comprehensive Design for Next-Generation Regional Aircraft

DLR Design Challenge 2024

Project Team:

Talha Sor
Yuvraj Salhan
Shuhan Yang
Constantin Koopman
Peter Faber
Prakhar Sharma

Submitted on July 21st, 2024

Institute of Aerospace Systems, RWTH Aachen University

Academic Support and Advisors

Univ.-Prof. Eike Stumpf
Laura Babetto, M. Sc.
Julian Callard, M.Sc.

Team Members

Talha Sor
M.Sc Aerospace Engineering
3. Semester

Constantin Koopman
M.Sc Aerospace Engineering
1. Semester

Peter Faber
M.Sc Aerospace Engineering
2. Semester

Yuvraj Salhan
M.Sc Aerospace Engineering
9. Semester

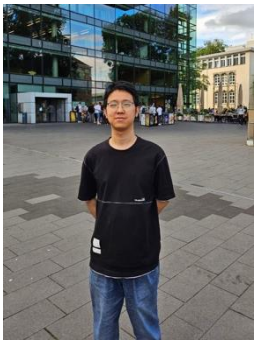

Shuhan Yang
M.Sc Aerospace Engineering
5. Semester

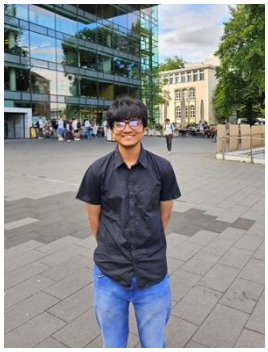

Prakhar Sharma
M.Sc Robotic Systems Engineering
4. Semester

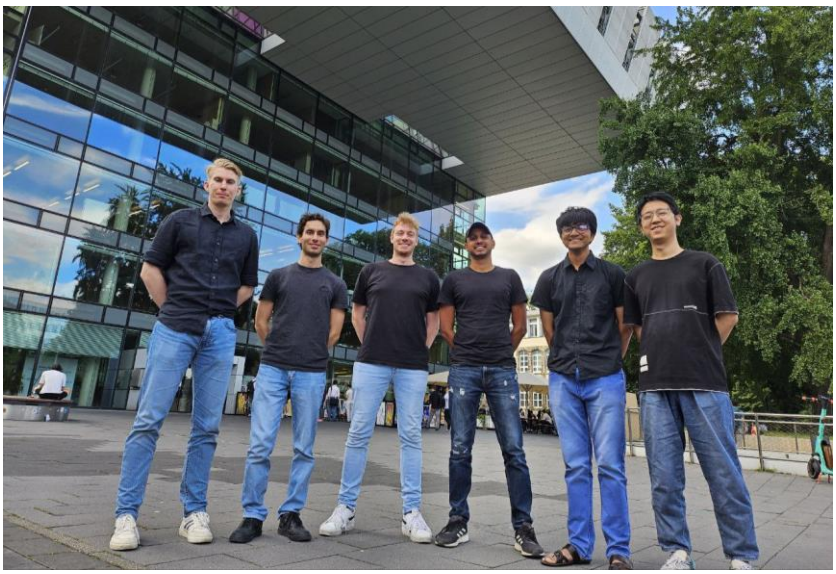

Abstract

This report is created as part of the DLR Design Challenge 2024 and presents EcoAir, a regional aircraft for 76 passengers with a planned entry into service in 2050. The report contains the initial design concept considerations, detailed technical data and a mission analysis for cost calculation. The ATR-72-600 serves as the reference and baseline aircraft for EcoAir.

During the conceptual design phase, the primary optimization goals were operational flexibility, direct operating costs and aircraft efficiency. The resulting design utilizes cryogenic, liquid hydrogen as the sole fuel source. The hydrogen is used in fuel cells to power the 4 main engines and an innovative boundary layer ingestion engine, which significantly enhances the aerodynamic efficiency. This enables EcoAir to operate entirely emission-free. A battery stores excess electrical energy from the fuel cells and supplies on-board systems, when needed. This guarantees optimal energy utilization.

Additional key features include sharkskin technology and hybrid laminar flow control on the wings, which reduce aerodynamic drag. Furthermore, foldable wingtips allow the EcoAir to be classified within a smaller category, providing access to numerous airports. Numerous airports. Another advantage of being classified in a smaller category also entails less restrictive operational requirements. These requirements are further reduced by a motorized nose landing wheel, which enables autonomous taxiing and thuseliminating the need for pushback trucks. Manufacturing costs are minimized by the windowless fuselage, while maintaining a passenger-friendly cabin with a wider layout and OLED screens projecting external views. The aircraft operates with a single pilot, supported by AI systems to maintain high safety standards and reduce crew costs.

These features collectively lead to significantly lower direct operating costs compared to the reference aircraft.

Dieser Bericht ist im Rahmen der DLR Design Challenge 2024 entstanden und stellt EcoAir vor, ein Kurzstreckenflugzeug für 76 Passagiere mit einer geplanten Indienststellung im Jahr 2050. Der Bericht zeigt die ersten Überlegungen zum Grundkonzept, detaillierte technische Daten und eine Missionsanalyse zur Kostenberechnung. EcoAir wird mit der ATR-72 als Referenz- und Basisflugzeug verglichen.

Bei der Konzeptionierung dienten die betriebliche Flexibilität, die direkten Betriebskosten und die Umweltauswirkungen als Optimierungsziele. Im Ergebnis wurde kryogener, flüssiger Wasserstoff der alleinige Treibstoff. Der Wasserstoff wird in Brennstoffzellen zum Antrieb der vier Haupttriebwerke und eines innovativen Hecktriebwerks zur Grenzschichtabsaugung verwendet, das den aerodynamischen Wirkungsgrad erheblich verbessert. Auf diese Weise arbeitet EcoAir völlig emissionsfrei. Eine Batterie speichert überschüssige elektrische Energie aus den Brennstoffzellen und leitet sie bei Bedarf an interne Systeme weiter. Dies garantiert eine optimale Energieausnutzung.

Schlüsselmerkmale sind die Sharkskin-Technologie und die hybride Laminarströmungskontrolle an den Flügeln, die den Luftwiderstand reduzieren. Darüber hinaus sind die Flügelspitzen faltbar, um eine günstigere Einstufung in eine kleinere Flugzeugkategorie zu erreichen, was den Zugang zu mehr Flughäfen. Ein weiterer Vorteil der Einstufung in eine kleinere Kategorie sind die weniger restriktiven betrieblichen Anforderungen. Diese Anforderungen werden durch ein motorisiertes Bugrad, das ein autonomes Rollen ermöglicht, noch weiter reduziert, so dass keine Pushback-Fahrzeuge mehr benötigt werden. Die Herstellungskosten werden durch den fensterlosen Rumpf niedrig gehalten, während die Passagierkabine mit einem freiräumigen Grundriss und OLED-Bildschirmen, die Außenansichten projizieren, angenehm gestaltet ist. Das Flugzeug wird von einem einzigen Piloten bedient, der von AI-basierten Systemen unterstützt wird, um hohe Sicherheitsstandards zu gewährleisten und die Kosten für die Besatzung zu senken.

Diese Merkmale führen zu deutlich niedrigeren direkten Betriebskosten im Vergleich zum Referenzflugzeug.

Contents

List of Figures

List of Tables

List of Symbols

Acronyms

AAA	Advanced Aircraft Analysis
AI	Artificial Intelligence
AR	Augmented Reality
AMC	Acceptable Means of Compliance
BLI	Boundary Layer Ingestion
C_cap	Capital Costs
C_crew	Crew Costs
C_fee	Costs through fee
CFRP	Carbon Fiber Reinforced Polymers
C_fuel	Fuel Costs
C_MC	Maintenance Costs
EIS	Entry Into Service
ESF	Engine Scaling Factor
FC	Fuel Cell
FC	Flight Cycle
GLA	Gust Manoeuvre Load
HEP	Hybrid Electric Propulsion
HLFC	Hybrid Laminar Flow Control
HSE	Human Systen Exploitation
ICE	Internal Combustion Engines
IFE	InFlight Entertainment
L/D	Lift to Drag
LH2	Liquid Hydrogen
MLA	Manoeuvre Load Alleviation
MLI	Multi-Layer Insulation
MTOM	Maximum Take Off Mass
OEM	Operating Empty Mass
OLED	Organic Light Emitting Diode
TS	Thrust Split
TSFC	Thrust Specific Fuel Consumption
T/O	Take Off
PSC	Power Saving Coefficient
FC	Fuel Cell
PEMFC	Proton Exchange Membrane Fuel Cell
HTP	Horizontal Tail Plane
HT-PEMFC	High Temperature Proton Exchange Membrane Fuel Cell
SAF	Sustainable Aircraft Fuel
SOFC	Solid Oxide Fuel Cell
SPO	Single-Pilot Operation
FC BoP	Fuel Cell Balance of Plant

PMU	Power Management Unit
VTP	Vertical Tail Plane

Symbols

α	[°]	Angle of Attack
B	[m]	Span
Γ	[°]	Dihedral Angle
l	[m]	Lever
P	[W]	Power

Indexes

0	Stationary point of operation, Equilibrium
o	Outward
W	Wind
v-tail	V-tail

1 Introduction

Rising concerns about climate change and the demand for city-to-city short haul travel emphasize the need for new regional aircraft. Solutions must be environmentally friendly and cost-effective to concur with existing train connections or motorized transport. To address these demands, new aircraft concepts must be developed. The EcoAir concept contains an innovative concept for futureproof city-to-city air travel while competing with other ground means of transport.

In Figure 1.1 the approach for the aircraft design study is given. The red line shows how the task [1] was solved, beginning in the task description. The process going thru each design step, to create demanded specifications. The green line shows the incorporation of key ideas for an optimal solution of the desired task. Used tools, being mostly literature research, MATLAB, and CAD to perform desired tasks are mapped to main use cases.

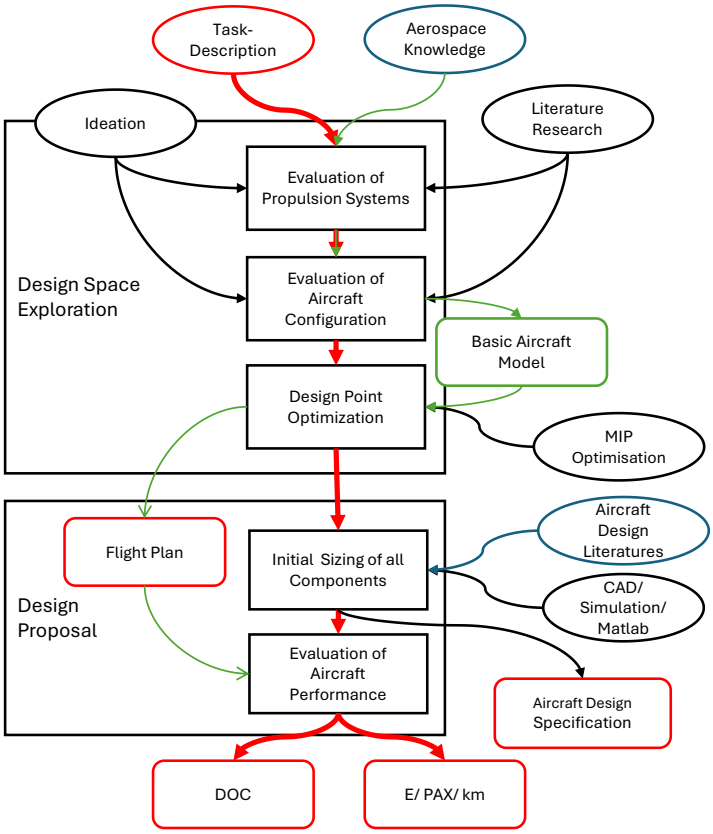

Figure 1.1: Overview of the report structure and design study. Round shapes are origins or tools rounded squares are results, while red colour is related to the task description and blue to the RWTH. Arrows show working processes.

Given the task description, fundamental aerospace knowledge from lectures and own ideation, the design space is defined. The design space is considered as large, because the task description does not directly consider only one special technology to be used or only some configurations as feasible. Within the boundaries of the task description, knowledge gathered in lecture was used to examine different technologies and build an understanding of feasible solutions. By conducting literature research, solutions could be collected, qualitative evaluated and joint to a preliminary quantitative aircraft model for numerical analysis. From this, a design point and an optimal flight plan is derived. Given that, a sizing process for the aircraft concept is started. The sizing process was firstly validated though a reference aircraft, namely the ATR-72. Afterwards, the validated process is used for sizing the proposed aircraft concept. Its performance were evaluated against the ATR-72 aircraft.

Established aircraft manufactures already provide solutions utilized by airlines, that offer flight routes as proposed by the task description. While these aircraft are designed for single mission performance on longer and more demanded routes, operation lacks efficiency and is more expensive and environmentally unfriendly.

Hence, the proposed design focuses firstly on optimization of multi-mission performance along with seeking for optimal costs and energy efficiency. In addition, given that new aviation technologies, such as innovative fuel for the propulsion system and material for the structure, already exist individually, the true innovation of

this design lies in how these technologies are integrated to meet the specific requirements of the desired mission. This way, a uniquely effective solution is proposed that maximizes performance and efficiency, while minimizing costs.

The report is divided into two main Sections: Chapter 2 examines the overall design space utilizing human system exploration methods and an optimization approach to select a design point. Chapter 3 presents the proposed design, while discussing remaining trade-offs. The evaluation of the aircraft concept is done in Chapter 4, encompassing the given optimization goals for Direct Operating Costs (DOC) and used energy per passenger per flight kilometre.

2 Design Space Exploration

Given the large design space, it is mandatory to dedicate considerable effort to exploring different design methodologies before solidifying an airplane configuration. By methodically strategizing the vast design space, the groundwork for later decisions in the actual design process is set. In the following Section, firstly feasible technologies are discussed, secondly, which one of them are applicable to our design and thirdly, how they perform on the desired mission. A human systems exploitation (HSE) method by Flemisch et al. [2] is adopted to clarify the posed questions with a structured approach supported by results. The proposed Innovation Turbine Model is shown in Figure 2.1. It is used as an iterative framework to explore general concepts, perform detailed analyses of the technologies in each concept and test the usability in a combined system. Each subsection of the Innovation Turbine Model consists of one full iteration and ends with a description of the discussed subsystem.

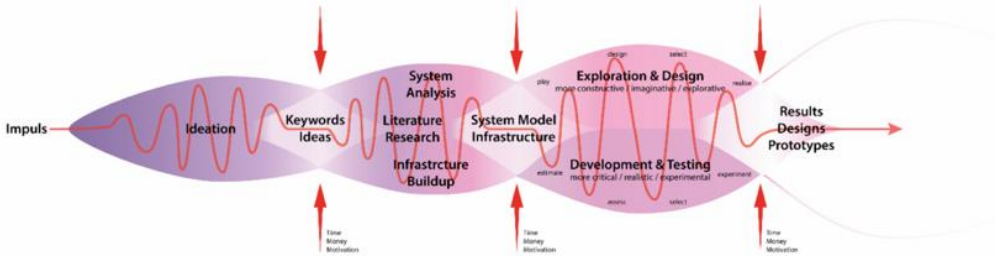

Figure 2.1: Innovation Turbine Model by Flemisch & Preutenbeck [2]

In the beginning of each iteration, the design space comprising innovative technologies and design solutions is described based on suitable aircraft concepts. The ideas are condensed to concepts, which will be further detailed. In the literature review and preliminary sizing, proposed concepts are evaluated and combined to a system model for conducting necessary trade-off studies. A presentation of summarized results related to the selected design concludes the evaluation.

The task description [1] incorporates an overall optimization goal, which is affected by preliminary design parameters. Because only one subsystem of the aircraft design is evaluated, a complete DOC or network energy calculation is not suitable. To overcome this, a parameterized equation for a reference aircraft has been derived from the approach further explained in Section 4.2. The Equation (2-1) is obtained by neglecting all constant sums and estimating the operating empty weight (OEW) always as half the maximum take-off mass (MTOW). The last term including the fuel cost is sized with the price for hydrogen. The units for range and MTOW are km and tons.

$$\min[9{,}5\,PAX + 1{,}1\,RANGE + 22{,}3\,MTOW + 3{,}4 \cdot 10^{-4} RANGE \cdot MTOW] \cdot FLIGHTS \qquad (2\text{-}1)$$

The propulsion system has the largest influence on the design as overall mass and range strongly depend on the Thrust specific fuel consumption (TSFC). Therefore, the first innovation turbine iteration is on exploring different propulsion systems with the focus on meeting mission requirements, while not including disadvantages, such as mass or drag penalties of some technologies. In the second iteration, various configurations based on Raymer's approach on unique aircraft concepts are explored. The influence on overall mass, wetted area or oval drag and trimmed maximum lift for different aircraft configurations is assessed and the values are compared to each other. The last iteration derives a flight plan for the given network of routes. Therefore, an optimal seating capacity and tank size is chosen with respect to given ranges and passenger requirements by the task description.

2.1 Evaluating Propulsion Systems

It is assumed that the given the three types of fuel, Sustainable Aviation Fuel (SAF), hydrogen, and electrical energy (electricity), are available in sufficient quantities. The projected prices are lower than estimates found in the literature as Holzen et al. [3] and Dahal et al. [4], rendering the consideration of other alternative fuels impractical. Such alternatives, like methanol or liquefied natural gas, would pose uncertain ecological benefits against certain economic and technological disadvantages. [4]

Hydrogen has been regarded as the fuel of the future for aviation since the 1950s, mainly because of its reduced emissions and therefore beneficial environmental impact. [5] Besides, its feasibility has been confirmed in numerous studies [6] [7] [8] [9] In contrast to hydrogen, SAF can be used as a drop-in fuel in the current aviation system without requiring major modifications. The task description only allows the use of SAF in a hybrid propulsion configuration. Several concepts for hybrid electric propulsion (HEP) exist [10] [11] [12] [13] [14] and appear reasonable for a regional aircraft. Despite the current challenges of using an all-electric aircraft for commercial purposes, [15] an all-electric propulsion system is evaluated because studies show its feasibility for a regional aircraft. [16] [17] [17] [18]

To evaluate propulsion alternatives, five comprehensive goals, divided in subgoals, are introduced, and weighted. Weighs are assessed by defining trade-offs between the goals. The alternative propulsion concepts and goals as well as weights and scores are listed in Table 2.1. The alternatives divide in pure hydrogen systems, hybrid systems and electric propulsion systems. Hydrogen requires implantation of new technologies and can be used for powering internal combustion engines (ICE) as well as fuel cells (FC). [6] Therefore, simplest drivetrains for booth concepts are observed. It's found that the higher efficiency of fuel cells is based on the electric motors generating thrust compared to ICEs. For hybrid configurations only parallel hybrid architectures with a power split between electric and combustion propulsors are considered. Parallel hybrid architectures couple combustion and electric propulsors in one device or simultaneous operation. Serial architectures utilize in difference ICEs to produce electricity for powering electric propulsors. Therefore, they reach nearly three times the weight compared to single fuel propulsion systems. [19] [20] For fully electric propulsion systems technologies like wing tip and over the wing distributed propulsors as well as boundary laver ingestion engines are evaluated. Despite the increase aerodynamic efficiency for these technologies, wing tip engines decrease positive effects by demanding a heavier structure. [21]

Table 2.1: Results of first weighted evaluation, Subgoals are evaluated from 0 to 3 with 3 as best

Goal	Sub Goals	Weight	SAF Hybrid	H2 Hybrid	H2 Turbines	H2 Fuel-Cell	Fully-Electric
Overall Cost	5	32%	0,50	0,63	0,57	0,53	0,72
Efficiency	4	32%	0,66	0,45	0,49	0,63	0,25
Sustainability	3	16%	0,22	0,31	0,27	0,39	0,43
Operations	1	3%	0,05	0,03	0,05	0,05	0,05
Safety	4	17%	0,43	0,34	0,29	0,34	0,43
		Score:	1,87	1,75	1,67	1,939	1,87

In addition to the weighted evaluation the impact of these technologies on overall mass reveals additional key points: Preliminary design calculations, [22] as well as above presented aircraft, as well as above presented aircraft concept studies indicate a significantly increased mass for utilizing batteries for energy storage. Therefore, fully electric aircraft configurations perform worse than others, according to equation (2-1). The same is applicable for SAF and batterie hybrid systems: either the airplane will be small and heavy, so many expensive flights are needed, or the hybrid factor approaches $\Phi=0$, [23] [24] so most of the energy comes from SAF. While LH2 has a higher specific energy and lower density than SAF, LH2 tanks are bigger and therefore heavier. With expected gravimetric efficiencies between 0,55 and 0,75 [25] [26] and estimated lower fuel masses and TSFC [27] [7] , only a slight increase of OEW for hydrogen configurations and a decreased MTOW due to fuel mass is expected.

Considering the weighted evaluation and further system exploration a hydrogen-based propulsion system for the aircraft is chosen. The high score of a FC propulsion system and possibilities of using distributed propulsors to increase aerodynamic efficiency makes FC the best option. Despite this, a hybrid concept containing LH2 ICE and FC is considered in the next Chapter. Because of the high thrust requirement for the steep take off compared to cruise and the need for possibly large thermal management systems to operate FCs, [6] an even power split during take-off, which is reduced during cruse to use the FC electricity for other systems. As the

feasibility depends on the aircraft configuration too, this trade-off cand be made here. The propulsion system evaluation is closed, choosing hydrogen for storing energy and a propulsion system with either only FC or a flight phase dependent power split of FC and ICE.

2.2 Evaluation of Airplane Configurations

After selecting the hydrogen propulsion system, various airplane configurations, targeting hydrogen integration and aerodynamic efficiency, are evaluated. Five aircraft configurations are selected and shown in Figure 2.2. When sizing the fuselage, it is important to ensure that the selected fuselage type can handle high climb and descent angles while maintaining efficient cruising performance.

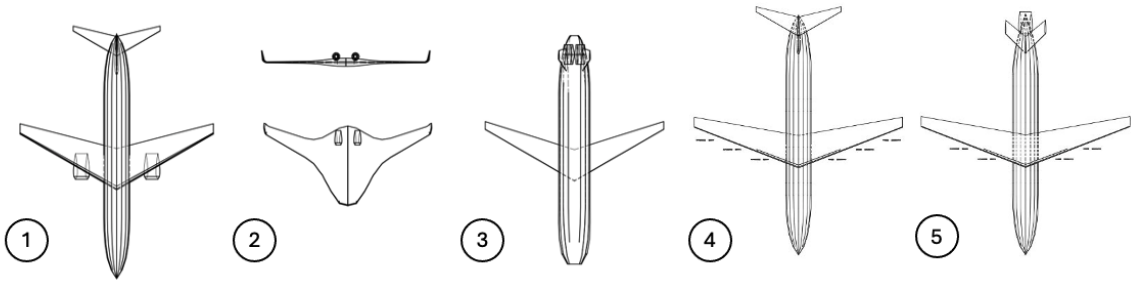

Figure 2.2: Five evaluated airplane configurations: 1 Conventional Layout (Conv), 2 Blended Wing Body (BWB), Double Bobble (BDF), 4 Distributed Propulsion (Distr.) 5 Hybrid Configuration (Hybrid)

The evaluated configurations are described as follows:

1. A standard configuration powered solely by fuel cells and electric propulsion can meet manoeuvring requirements. Moreover, the integration of fuel cells and electric fans as designated propulsion system is feasible. [16] However, it might require lower wing loading during cruise to fulfil the high climb and descend angles, which could lead to an increase in structural weight. [22]

2. Blended Wing Body (BWB) configurations offer a high aerodynamic efficiency during cruise flight, but the overall mass compared to standard configurations is increased. [28] The propulsion is accomplished by two ducted fans installed in the rear section of the aircraft in the place of the V-tail. [29] A downside might be the passenger acceptance and convince as well as boarding procedures. [30]

3. Lifting bodies (LB), such as the Double Bubble Fuselage (DBF), [31] are notable for their reduced trim drag, which benefits the take-off and landing and increases aerodynamic efficiency. [32] The wider body offers accommodation for a double aisle seating configuration enhancing efficiency in boarding procedures. [33]

4. Distributed fans over the wing reduce overall drag and permit high climb angles. [10] Due to the larger propeller diameter, a high wing and a T- tail is considered.

5. Additionally, a tube-and-wing configuration is considered. In contrast to the conventional layout, the integration of a turbine at the rear is considered. This can be coupled either with wingtip engines or distributed propulsion on the wings. The engine in the rear part provides most of the thrust for the cruise flight, while it is supplemented by the fuel cell-driven- electric engines during take-off and engine failures. Even boundary layer Ingestion can be utilised. [34]

A weighted evaluation as in Section 2.1. is performed, regarding five goals, containing several subgoals. The alternatives, goals, weights, and scores are listed in table 2.2. The passenger goal includes comfort and acceptance of new technologies. Performance indicates all aerodynamic, flight-mechanic and mass considerations, while certification includes concurrence with CS-25 as well as stability and controllability. The usability indicates the possibility of integration needed technology and the feasibility for the desired missions.

While LBs and BWBs do not reduce the wetted area, they do offer drag reduction of over 6% but only for an increased weight of around 13%. [32] High aerodynamic loads during take-off and landing require more structural support for lift-generating surfaces, further increasing the mass for DB and BWB configuration. [29]

Table 2.2: Results of second weighted evaluation. Subgoals are evaluated from 0 to 3 with 3 as best

Goal	Sub Goals		1 Conv.	2 BWB	3 DBF	4 Disstr.	5 Hybrid
Passenger	2	16%	3,00	1	2	3	3
Performance	3	27%	2,06	1,80	1,90	2,70	2,60
Certification	2	19%	2,57	0,57	1,57	2,57	2,14
Usability	2	14%	1,80	2,20	2,60	1,80	1,40
Cost	2	24%	2,33	0,67	1,67	3,00	1,33
		Score:	2,43	1,21	1,89	2,68	2,35

Placing engines at the rear can reduce the overall drag and provides the opportunity to utilize Boundary Layer Ingestion (BLI) technology to further reduce drag. [35] [34] [36]Looking at possible empennage configurations T-tails are bigger compared to conventional tails, which are in turn bigger than V-tails. This increase in size contributes to gains in both weight and wetted area, which decreases the overall performance. [22]

For choosing a final configuration, the performance and cost characteristics from the distributed propulsion configuration are combined with a V-tail and an electric BLI engine in the back. The aircraft is powered by FCs, eliminating certification uncertainties regarding engine failures due to power split between ICE and FC.

2.3 Evaluation of a Design Point

After the preliminary evaluation of possible potential technologies and the selection of the best available options solutions, the design process for the aircraft follows. The Top-Level Aircraft Requirements (TLARs) are not entirely defined in the task description. In this Section, the TLAR are finalized by investigating at the design range and passenger capacity and summarize them at the end.

Significant differences in the specified routes necessitate various operational points, which can be already considered in the preliminary design stage. [37] [38] Since a greater range is achieved by a lower payload while maintaining the MTOW, an optimal mission plan must be defined. Introducing a layover can significantly shorten the maximum required range, but it necessitates two take-offs and landings, which is not beneficial especially for regional aircraft. [39] To deal with these considerations, an optimization model to set a flight plan (Table 4.2, p. 24) is derived as well as an optimal design mission. The optimization approach consists of three steps which are iterated until convergence of the optimization value based on DOC and total flight energy is reached.

1. To select a design operating point, an initial aircraft is conceptualized using preliminary design formulas by D. Raymer. [22] For weight estimation, a simple mass balance comprising payload, fuel weight, and empty weight is used. The empty weight is estimated based on mass fraction regression for twin-engine turboprop aircraft. The fuel estimate assumes phases of take-off, climb, cruise, and landing as flight phases, with the cruise phase corresponding to the specified route lengths. This preliminary design depends therefore solely on SFC=4,14E-6 kg/(N·s) and cruise speed v=130 m/s.

2. Based on the first estimation, fuel masses are obtained for a 5% higher and 15% lower range. While keeping maintaining the OEW and MTOW constant, the payload capacity for both ranges is calculated. The calculations are derived from the Breguet equation. [27] The resulting values provide a trade-off factor (Eq. 2-2), representing the gained range per passenger reduction.

$$Coff = |R_1 - R_2|/|PAX_1 - PAX_2| \qquad 2\text{-}2$$

3. We use the obtained parameters for mass, range, payload, and the trade-off factor in a Mixed-Integer Optimization assignment program. The optimization objective is given in Eq. 1. To consider the influence of intermediate stops, a penalty factor for each stop in the flight plan is added. The constraints are based on an assignment problem by G. Danzig. [40] The modified and added constraints are explained in the following. The remaining constraints regarding slot capacity and model-specific optimizations are not provided here.

$$FLIGHTS_i \cdot SEATS_i \geq P_i \qquad 2\text{-}3$$

$$RANGE + (PAX - SEATS_i) \cdot Coff \geq D_{i,x} \quad 2\text{-}4$$

$$PAX - SEATS_i \leq 0{,}25 \cdot PAX \quad 2\text{-}5$$

The closing constraint (Eq. 2-3) ensures for every route i that every passenger P_i has an assigned seat. Due to the assignment of two variables and the nature of the optimization function, the problem is no longer linear. The aircraft must be capable of flying every distance. This is due to either the design point range or a lower payload capacity (Eq. 2-4). Different distances are used, depending on weather intermediate stops are made or not. The model for the trade-of factor and the filling requirements of the LH2 tanks ensure that only 25 % of the spaces are empty (Eq. 2-5).

The optimization concludes with an optimal design point for range and payload in Table 2.3, estimates for MTOW, OEW and fuel mass and a flight plan for one week (Table 4.2, p. 24). This comprehensive analysis ensures that the aircraft design is optimized for efficiency, operational flexibility, and cost-effectiveness, aligning with the goal of developing a future regional aircraft configuration that meets all specified requirements. In the upcoming design process, the following TLARs are used:

Table 2.3: Summary of TLARs and Sources

TLAR	Value	Unit	Origin
Range	900	km	Chap 2.3
Payload	76	Passengers a 95 kg	Chap 2.3
Cruise Mach number	0,42		Ref. Aircraft
Cruise altitude	7475	m	Ref. Aircraft
Take off distance	1315	m	Task description
Landing distance	915	m	Task description
Approach speed	33	kts	Ref. Aircraft
Time to climb	30	min	[22] [41]
Diversion range	250	km	Task description

3 Proposed Design – Technical Data

This Chapter presents a comprehensive overview of the proposed aircraft design, which incorporates several innovative features aimed at enhancing operational efficiency and reducing costs. As illustrated in Figure 3.1, EcoAir integrates advanced technologies, including foldable wingtips for classification within a smaller aircraft category, a motorized nose landing wheel for autonomous taxiing, a FC propulsion system utilizing distributed propellers and a BLI engine. These features and additional aerodynamic enhancements collectively contribute to a design that maximizes efficiency, reduces maintenance and manufacturing costs and broadens the operational capabilities of the aircraft. The design and integration into the overall system is presented, and the final considerations determining the selection of the less influential subsystems are explained.

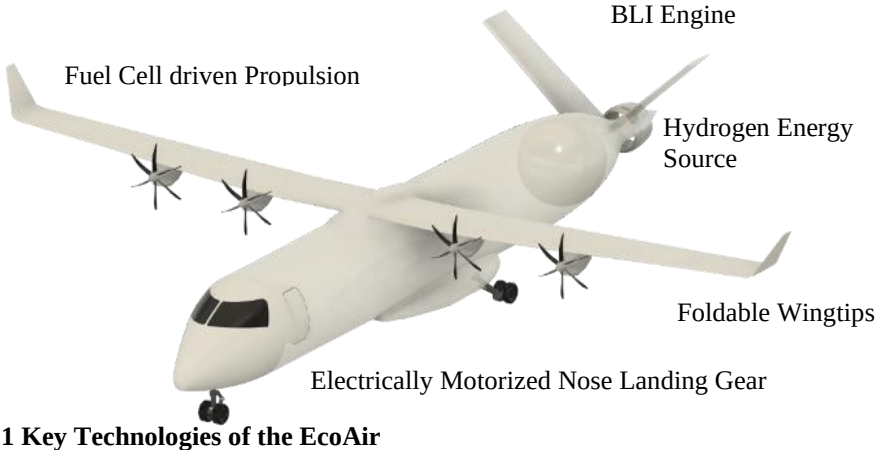

Figure 3.1 Key Technologies of the EcoAir

The reference aircraft for this regional aircraft design is the ATR 72-600 due to its turboprop-powered propulsion system with comparable range and passenger requirements to EcoAir. The ATR 72-600's proven track record, cost-effectiveness, and fuel efficiency made it an ideal baseline for adapting and enhancing it to meet new design requirements [42]. Therefore, adjustments were made to the ATR 72-600 to align it with the task description and performance requirements of the proposed design. The performed calculations and aircraft design methodology are based on the principles outlined in well-established aircraft design literatures [22] [43] [41]. Furthermore, by first performing the conceptual design calculations on the ATR 72-600, it was possible to validate the applied aircraft design methodology. Based on this methodology, an initial sizing was performed, identifying sizing constraints and allowing for the selection of an optimal design point, as shown in Figure 3.2.

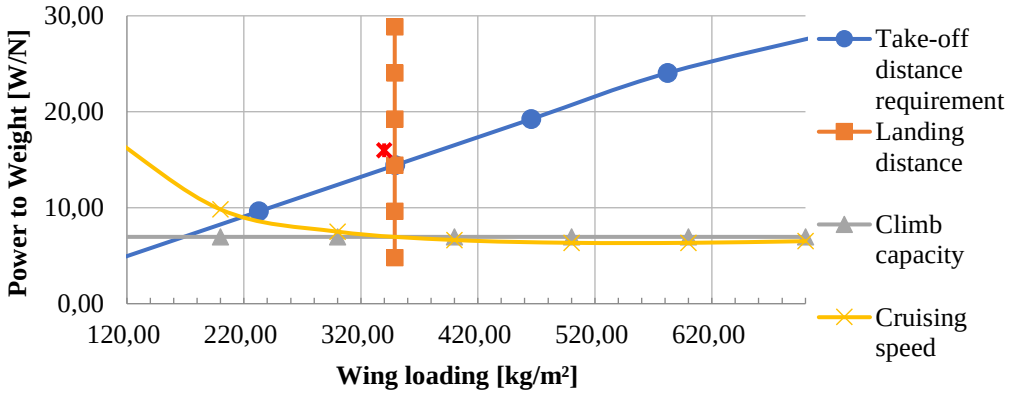

Figure 3.2: Chosen Design Point of EcoAir

3.1 Fuselage

This Chapter gives a detailed overview of the biggest part of the aircraft. It consists of two further categories: fuselage layout and cabin, where the structure, material and the cabin compartments will be discussed.

3.1.1 Fuselage Layout

The total length of 28.45m and the main circular tube with an outer cross-section diameter of 3.5m is considered due to increasing passenger comfort in cabin and placement of the tank in the tail area. The increased demand for space to accommodate propulsion systems, luggage, and landing gears calls for a bigger fuselage. During the design and material choice for EcoAir, a special focus is kept on advanced technologies and cost reduction manufacturing processes. The use of composite materials and structural design principles are therefore highly considered. Making the main body section, the fuselage of this aircraft accommodates pilots, passengers, crew, the main landing gears, luggage, and the fuel tank. The detailed length are shown in figure Figure 3.3.

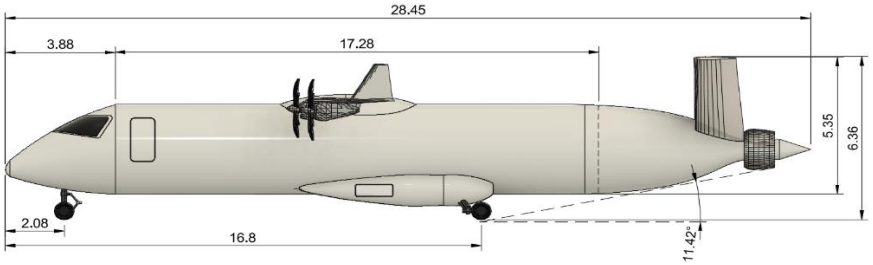

Figure 3.3: Side View of EcoAir

The Semi-monocoque carbon fibre reinforced polymers (CFRP) structure is used, due to the properties such as higher strength to weight ratio, significantly higher fatigue resistance in comparison to aluminum alloys and corrosion resistance [44]. This allows 20%-30% reduction in aircraft weight [45]. On the other hand, it lowers the operational cost and global environment impact. CFRP covers the most outer visible part of the aircraft talking about Fuselage, and the tail with the help of mounted stiffener and integral stringers [46]. The cockpit area, crossbeam and cabin floor is made with aluminum-lithium alloy can be seen in Figure 3.4.

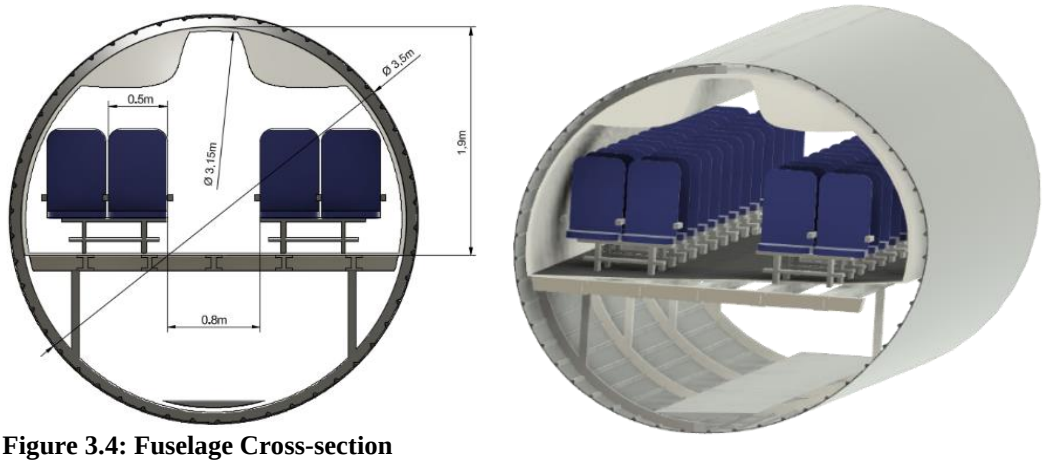

Figure 3.4: Fuselage Cross-section

A further effort to make the aircraft more economical and reduce emissions is done by minimizing the losses due to wall and the microscopic vortices interaction. A surface film named AeroSHARK, with riblets measuring around 50 micrometres that mimics sharkskin's characteristics and aerodynamics is applied on the fuselage and wings of the aircraft aligned with the desired airflow direction [47].Using an alternative way to reduce structural mass, a windowless cabin concept is introduced into EcoAir. That way, the fuselage design is simplified. Therefore, removal of all the windows except for the door and emergency exits [45].

The landing gears support aircraft during ground operations, take off and the landing. Due to the high wing configuration, they are placed inside the lower fuselage, with the thought of extra podded shape on the sides. The required least tail strike angle 11.4° is maintained. Another cut out is made below the cockpit to mount front landing gears. For effective ground operation an electric motor is placed in the front landing gear. This allows for taxing without engine thrust and no need for a pushback, utilizing electric energy of the FC for the landing gear instead of the electric propulsors.

3.1.2 Cabin Interior

Passengers aboard EcoAir's wide single-aisle single-class cabin appreciate increased personal space, larger seats, and ample overhead storage for their belongings. The cabin is 18m long and inner diameter of 3.15m, offering 76 passenger and an 8cm longer seat width as compared to the reference aircraft. Two seats for the cabin crew are placed, one in the front and one at the rear side. A toilet is placed in the front right area of the cabin as shown in Figure 3.5. The cabin is designed to target the reduction of costs, weight, and environmental impacts. A sustainable cabin design with efficient structures such as fine 3D printing plastics, sustainable cabin materials such as bioplastics, bio-composite reinforcements with sustainable cabin electronics like Solid-state batteries, and with an extra key factor of recycling for example- Li-ion battery recycling, textile waste recycling and plastics recyclingis applied. [48]

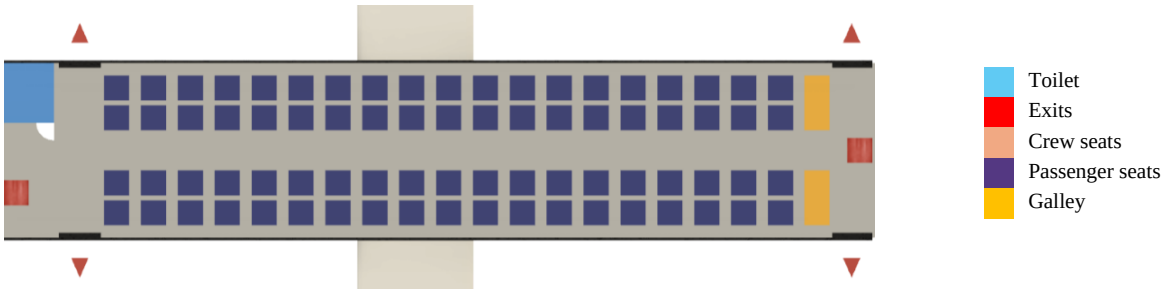

Figure 3.5: Cabin Layout

Cameras and display systems are introduced to overcome the only limitation of the proposed design: the lack of external field view. Multiple cameras are mounted outside the fuselage to capture the external view at real time. The positions were chosen in a way that they do not affect the aerodynamics. The footing is projected on a window shaped screen inside the aircraft [49]. For an increased passenger entertainment experience, each seat back is fitted with Super-thin large organic light-emitting diode (OLED) flexible curved screens and smartphone compatible for the inflight entertainment (IFE) displays interactive screens. They have been chosen for their light weight, and less electricity consumption.

3.1.3 Hydrogen Tank Integration and Design

The design and integration of a fuel storage, control and distribution system is one of the main challenges of hydrogen-powered aircraft design as it heavily impacts the aircraft's overall weight and performance. The following Chapter shows detailed solutions on how EcoAir's fuel systems are integrated.

Possible storage methods must be evaluated regarding safety, gravimetric and volumetric efficiency as main criteria. The latter two are mainly influenced by the state in which the hydrogen is carried. Broadly speaking, there are three ways to store hydrogen as a fuel: a high pressurized gas, a cryo-compressed gas or in liquid state. As shown by Verstraete liquid hydrogen tanks have the highest gravimetric efficiency and need the least amount of volume. [50] The comparatively speaking low tank mass is required due to lower internal pressure than in gaseous storage systems. Therefore, a LH2 tank is designed in the following.

Table 3.1: Possible positions for LH2 storage [51]

Internal	External
Rear of cabin	Above fuselage
Front of cabin	Under-wing
Top of cabin	Over-wing
Middle (between forward and aft cabin)	Between joined wing
Below cabin	Conformal

Using LH2 as a commercial aircraft fuel, losses due to boil-off inside the tank must be as low as possible. To prevent boil-off inside a cryogenic tank, the tank shape must optimize the ratio between volume and surface area. Furthermore, an increase in this ratio results in an increased gravimetric and volumetric efficiency. [50] While spherical tanks are more challenging to manufacture and have a larger frontal surface area than cylindrical tanks, they offer the optimal volume-to-surface ratio. [52] Moreover, the gravimetric efficiency benefits further from the lower pressure in spherical tanks; hence, fewer wall material is needed. For the reasons given, a spherical tank is chosen for EcoAir. This is done first because manufacturing costs are expected to decrease until entry into service and, second, the increased frontal area will not induce additional drag the way it is placed as described in the following.

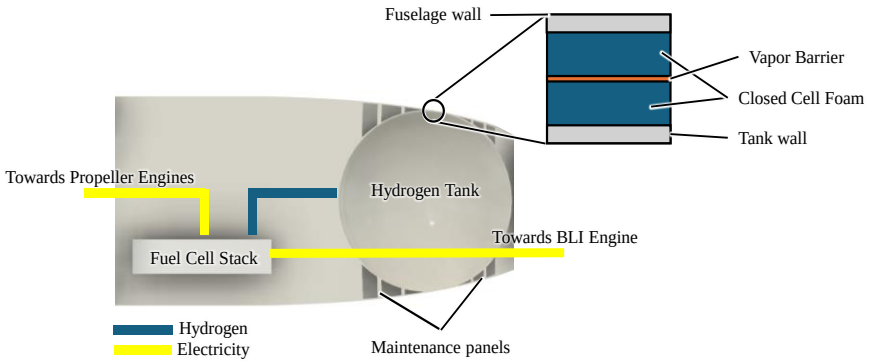

Figure 3.6: Schematic representation of the LH2 storage and distribution

As shown by Rompokos et al., there are mainly ten possible locations for LH2 storage, which are shown in Table 3.1. [51] External tank systems commonly show disadvantages in aerodynamic behaviour as they increase the wetted area and therefore drag. [53] The same issues apply to internal tanks on top of the cabin. Covers must be installed on top of the fuselage furtherly increasing weight. [51] Additionally, external tanks tend to have larger wall thickness and, in turns, masses. [54] Therefore, these configurations are excluded, and an internal allocation is chosen.

From a safety perspective, the tank must not be placed inside the pressurized cabin. [53] Additionally, the cargo storage department should not be removed, leaving the rear or front of the cabin as the remaining possible areas. Lastly, placing the tank closer to the engines and fuel cells results in shorter fuel lines or shorter cables, which are favourable as they minimize failure possibilities. Overall, a spherical tank at the rear end of the aircraft is deemed to be the optimal solution for EcoAir. Figure 3.6 shows the fuel tank and distribution systems.

Regarding insulation options, there are four main solutions for hydrogen tank walls: foams, aerogels, vacuum, and multi-layer insulation (MLI). [52] Vacuum is unsuitable for aviation due to the complexity of maintaining it and the safety risks in case of a leak. MLI effectively reduces heat transfer with multiple reflective layers but requires vacuum isolation and, therefore, it suffers from the same disadvantages. Aerogels offer excellent insulation but cannot bear mechanical loads, therefore requiring additional tank mass, and are not well-researched. [50]

The design of the insulating tank wall is adapted from Verstraete's proposals for a single wall construction as shown in 4. According to Verstraete, the tank wall for liquid hydrogen storage is constructed with an inner layer made of high-strength, low-weight materials to withstand low temperatures and pressure. [54] Aluminium is an ideal candidate. Although foams have moderate thermal conductivity and can be damaged external influence, they are considered the best compromise in this study. A closed-cell polyurethane foam is applied to the exterior of the inner tank wall, which absorbs mechanical loads and provides further insulation. This way the inner wall is relieved and the reduced stress results in decreased thickness and therefore mass. Besides, no second structural wall is required [50]. The only purpose of the outer wall is to protect the foam from damage. The optimal thickness of the isolation without a frameworks 7mm according to Silberhorn [53]. The overall mass can be derived from the desired full mass and the predicted gravimetric efficiency of 0,6 by 2050 [55]. The most important geometric quantities are summarized in Table 3.2 below.

Table 3.2: Parameters of the LH2 tank

Parameter	Value	Unit
Inner Volume	14,135	m^3
Tank empty mass	491,26	kg
Tank and fuel mass	1603,6	kg
Isolation thickness	0,007	m

The tank is effortless to maintain through the integral design as the heatshield solely needs to be removed and not the entire tank. [50] Wedge-shaped panels fill the gap between the hull and the spherical shape of the tank at the point where the tank does not overlap directly with the fuselage, as shown in Figure 3.6. Manholes are intended for maintenance in the intermediate spaces, through which the tank can be reached from the inside. In addition to maintenance work, ground handling also includes refuelling. In terms of safety, the same kind of risks are expected compared to the current handling of kerosene. [56]. But order to keep these risks equally low, safety systems must be adapted to hydrogen. These include, for example, the installation of gaseous hydrogen detectors. [57]

3.2 Propulsion System

The propulsion systems of modern aircraft are evolving rapidly, particularly with the development of electric BLI engines and distributed propeller engines. These advancements promise significant improvements in efficiency, fuel consumption, and overall aircraft performance. [58] [59] The proposed propulsion system leverages the advantages of Proton-Exchange Membrane Fuel Cells (PEMFC) and batteries to deliver a highly efficient and reliable power source for EcoAir. This system is designed to operate efficiently across a wide range of conditions, ensuring optimal performance during all flight phases. The detailed architecture and functionality of this innovative propulsion system are explored in this Chapter.

3.2.1 Electric BLI – and Propeller Engines

A BLI engine, positioned at the aft fuselage, is designed to ingest the airframe's boundary layer flow. This configuration leads to several benefits, including power savings, a slight increase in the Lift-to-Drag (L/D) ratio, and a reduction in TSFC. [58] [60]

The use of an electric drive instead of an internal combustion engine greatly simplifies the aero-structural integration of the aft-fuselage propulsor shown in Figure 3.7. This approach allows the BLI propulsive device to be installed at the very aft end of the fuselage, maximizing the wake-filling effect achievable from BLI while minimizing vibrations and losses due to shear flow on the fuselage aft cone. Additionally, the BLI engine was positioned at the centre of the fuselage diameter to ensure uniform airflow at the nacelle inlet [61]. The precise longitudinal position of the BLI engine was determined by interpolating data from other fuselage fan configurations [58]. As a result, the BLI engine inlet is near the empennage. This means that the additional impact of the tail wake flow on the BLI fan needs to be considered. However, this design offers the aforementioned advantages and does not enlarge the tail section of the aircraft. [62]

Another advantage of this configuration is that the empennage loads are transferred directly to the fuselage, bypassing the fan nacelle. This results in simpler manufacturing and maintenance, as well as a lighter nacelle structure compared to integrating a BLI engine into the empennage. [62]

The intake struts are placed behind the fan since the struts can function as guide vanes without distorting the air inflow before the fan. The motor is located at the tail end, making optimal use of the available space.

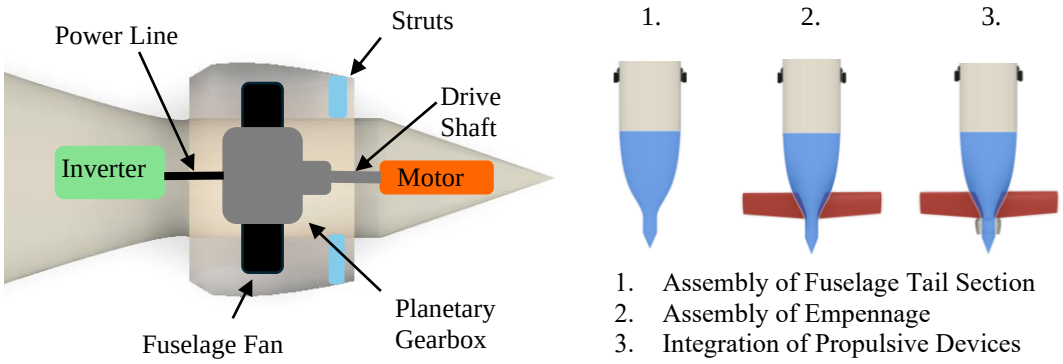

Figure 3.7: BLI Engine Design Layout (left) and its Structural Integration (right)

An additional benefit of this configuration is the reduction in the number of required propeller engines under the wings. Without the BLI engine, six instead of four propeller engines would be needed, thus reducing the overall number of engines by one and cutting costs. Having four engines distributed along the wing already demonstrates significant advantages. Firstly, the critical sizing factor is no longer the one-engine-inoperative scenario, allowing for a reduction in power requirements [63], as confirmed by calculations for EcoAir as well. Secondly, the drag reduction achieved through distributed propeller engines along the wingspan also applies in this concept. Keller, D. supports this benefit, attributing it to the magnitude and orientation of local force vectors and the less inhomogeneous propeller load distributions impacting the main wing aerodynamics that is observable even with a total of four propellers [64]. Compared to the baseline aircraft configuration, the inner engines are further from the fuselage to avoid disrupting the BLI inflow.

3.2.2 Engine Specifications

The TSFC and specifications for the propeller engines are based on Fly Zero's Carbon Emission aircraft concept, whereas for the BLI engine the values had to be interpolated from other conceptual fuselage fan designs and adjusted to EcoAir's propulsion system [65] [58]. Both engine types were then downscaled to the aircraft's specific power requirement with an Engine Scaling Factor (ESF) close to 1.

The only dimension of the propeller engine that is larger than the ATR 72's engine is the engine volume, due to the need of larger air inlets for the heat management of the FCs, which is described in more detail in the next Sub [66].

For the BLI engine a smaller fan diameter is chosen compared to other fuselage fan designs. [58] This choice is driven by the higher yield in the Power Saving Coefficient (PSC), which quantifies the relative benefit of BLI compared to an engine without BLI, as seen in equation (3-1). [61]

$$PSC = \frac{P_{shaft} - P_{shaft-BLI}}{P_{shaft}} \quad \text{(3-1) [58]}$$

Furthermore, opting for a larger fan diameter introduces a weight penalty due to the larger nacelle and can result in some flow being ingested directly from the freestream rather than the fuselage wake. This is undesirable as it increases non-uniformity in the fan-face total pressure distribution, leading to more inlet distortions. [61]

Conclusively, the overall Thrust Split (TS), meaning the relative net force provided by the BLI propulsors compared to the aircraft's overall thrust, has been determined to be 0,2. This value is ideal for the proposed configuration, since it limits the engine size while maximizing the BLI effect [58]. After an iteration of different TSs and engine dimensions to get the optimal PSC, a PSC of 7% is assumed. Although other fuselage fan concepts claim higher PSCs with lower TS, the decision for the PSC was constrained by the lack of complex computational models for aerodynamic simulations across all flight segments and matching schemes that consider airframe/engine interactions comprehensively [67]. Consequently, the chosen PSC results in an estimated 5, 4.5 and 3 percent of reduction in TSFC, fuel burn and L/D, respectively [67] [60]. A comprehensive overview of the Propeller- and BLI engine data is presented in Table 3.3.

Table 3.3: Propeller- and BLI Engine Data

Propeller Engine		**BLI Engine**	
Length [m]	1,6	Length [m]	1,4
Nacelle Diameter [m]	0,95	Nacelle Diameter [m]	1,5
Propeller Diameter [m]	2,3	PSC [%]	5
T/O Power [kW]	6450	T/O Power [kW]	6450
Thrust Split [%]	20	TSFC [kg/Ns]	4,37*10^-6

3.2.3 Propulsion System Architecture

The propulsion system of EcoAir integrates several critical components to ensure efficient and reliable operation. At the core of the propulsion system are the FCs, while the auxiliary systems that ensure the safe operation of the FCs are collectively known as the FC's Balance of Plant (BoP) [68]. For the FCs itself a choice had to be made between several FC types, whereas two FC types are most suitable for aircraft applications. [69] These are the Solid Oxide FCs (SOFC) and PEMFC [70].

SOFCs require preheating to a certain operating temperature before they can function effectively. This preheating is typically achieved using electrical heating elements or other methods, increasing weight. On the other hand, PEMFCs operate at lower temperatures and do not need an extended preheating phase. Furthermore, PEMFCs have faster startup times, better load-following capabilities, lighter weight, and higher tolerance for on/off cycles. [70] Consequently, PEMFCs have been chosen over SOFCs. With the advent of major improvements of PEMFCs in the aviation sector, High Temperature PEMFCs (HT-PEMFC) are expected to enter the market in 2050 and further increase the performance of the FCs. Additionally, the higher operating temperature of the HT-PEMFC allows for easier heat dissipation of the FC into the ambient environment due to the higher temperature differential, which is why HT-PEMFCs were chosen. [70] [71]

For the placing of the FCs, it was decided to not integrate them inside the pylon or engine. This decision was made, because longer hydrogen lines would be required, posing a safety risk and resulting in more energy loss due to heat convection compared to electric power transmission. [70]

To provide the necessary oxygen for the operation of the FCs, air inlets are integrated into the propeller engines to ensure a continuous supply of air. The air supply system includes a preconditioning unit with humidifiers to ensure the air reaching the FCs is appropriately humidified and controlled for pressure and flow rate. The flow rates are controlled to achieve an appropriate stoichiometric ratio of reactants, so that the FC does not have a shortage or excess of oxygen, which could affect the efficiency and lifetime of the FCs. [72]

As a result of the electrochemical reactions inside the FCs, exhaust water is produced, which is either stored in the aircraft’s water tank or released during flight [69]. Storing the water is crucial during Take-Off (T/O) and landing to prevent runway friction issues caused by water discharge. It not also ensures operational safety but also contributes to the aircraft's overall efficiency as the water can be repurposed for various applications such as for potable water, toilet water and humidification of the cabin air. [71]

Another inadvertent byproduct of the FC is heat. Contrary to the water storage system, the heat generated by the FCs is not used for synergistic effects, as it is not a reliable source for on-demand heat requirements like anti-icing systems. To avoid overheating of the FCs, a cooling system is essential for the operation of FC-driven propulsion systems, especially considering the wide range of ambient temperatures EcoAir may encounter [72]. The cooling system collects heat generated by the FC stack by a liquid coolant that circulates through channels in the FC stack. The heated coolant passes through heat exchangers placed inside each of the 4 propeller engines’ nacelles. The heat exchangers located inside each nacelle facilitate the transfer of heat from the coolant to the airflow coming from the air inlet, which also supplies the necessary airflow for the electrochemical reactions in the FCs. By cooling the heat exchangers with air instead of liquid coolants, the cooling system’s weight can be reduced significantly [70]. The design of the nacelle ensures sufficient airflow over the heat exchanger, as illustrated in Figure 3.8. Positioning additional heat exchangers inside the wing could enhance the cooling efficiency due to the high-speed airflow around wings during flight. However, this would result in a warmer wing surface, making the boundary layer of the wings more unstable and prone to turbulent transitioning. [73] Therefore, the additional heat exchangers are strategically positioned within the fuselage.

After the heat is transferred to the airflow, the now-cooled coolant is recirculated back to the FC stacks to absorb more heat, thus maintaining the continuous cooling cycle. The cooling system also includes a coolant tank that accommodates the expansion and contraction of the coolant medium in response to various

temperature conditions. This ensures the cooling system functions effectively across various operating environments.

The final main component of the propulsion system are the inverters and DC-DC converters. The DC-DC converter is used to regulate the voltage output from the FCs to match the required levels for different aircraft systems, while an inverter converts the DC electricity produced by the FCs into AC electricity to power the aircraft's motors. [62] [74] The inverters are placed in the pylon of the propeller engine and in the aft for the BLI engine, whereas the DC-DC converters are next to the FC stacks. This setup avoids the need for long AC cables, which can be problematic for the following reasons. Firstly, synchronizing electric machines to an AC grid can be catastrophic for the aircraft due to the limited experience with system stability in such small AC grids. Additionally, AC grids require larger cables to transport reactive power, necessitating larger electric machines to deliver this power.

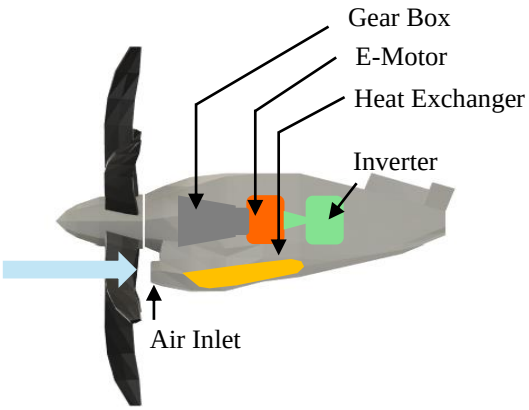

Figure 3.8: Interior View of the Propeller Nacelle

In the proposed aircraft systems architecture, a battery is employed as well. The main task of the battery is providing aidance to the FCs and powering all non-propulsive components, like the electric motors in the nose wheel, during all mission segments except cruise. This strategy maintains a consistent power requirement for the FCs throughout each flight segment. During cruise flight, the FCs generate surplus power, which is then utilized to power the non-propulsive systems and to recharge the batteries. This configuration allows the FC to operate under ideal conditions, even during take-off, thereby enhancing efficiency and extending lifespan while reducing costs. [75] In order to facilitate flexible load balancing between the FCs and the battery, a Power Management Unit (PMU) is used, ensuring optimal FC operation and managing power fluctuations that may arise, particularly due to inflow distortions of the BLI engine during different flight phases. [75]

Conclusively, the electric propulsion system architecture is illustrated in Figure 3.9 showcasing the integration and layout of all components. The propulsion system architecture is built in a modular design, allowing the replacement of parts of the system, as well as enabling easy maintenance of the system components under the fuselage and inside the engines. The interchangeability of the system components is necessary as e.g. the FC generally has a shorter life span than the aircraft itself. [68]

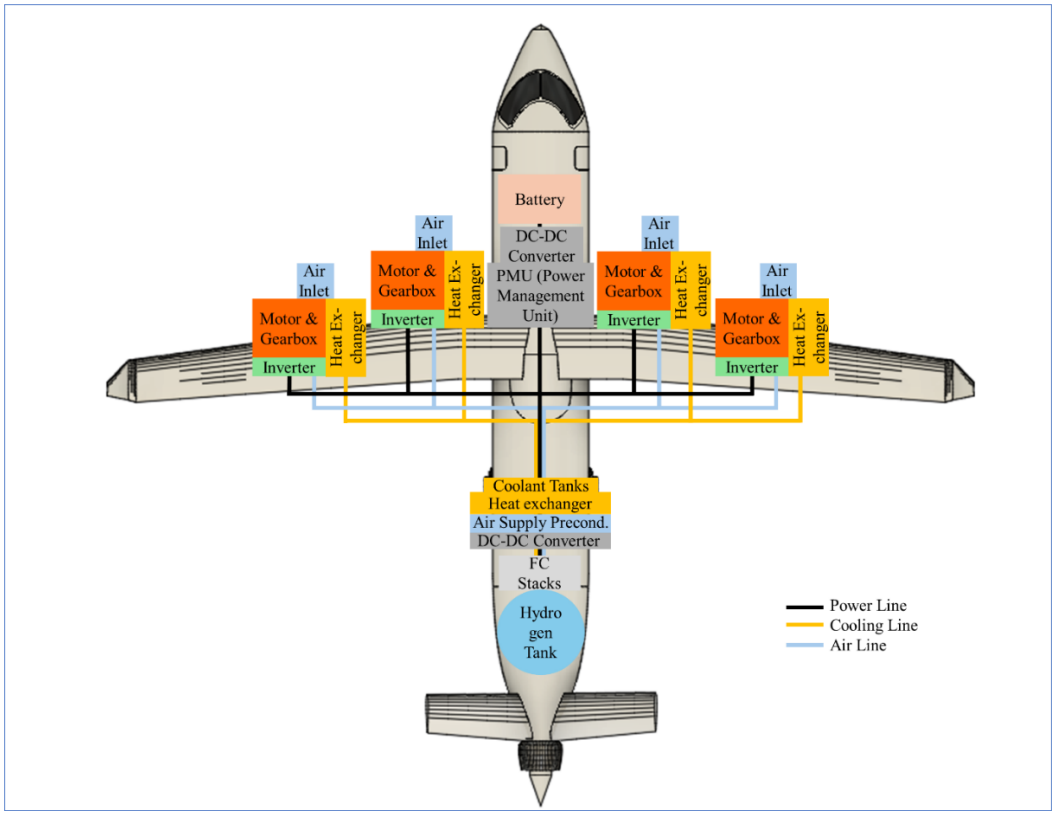

Figure 3.9: Electric Propulsion System Architecture

To better understand the interplay between FCs and the battery, the battery and its function is further explained. The battery supports the FCs by enabling the startup of the FC's chemical reaction process. The battery does this by powering two small fans integrated symmetrically inside the fuselage at the beginning of the elongated landing gear compartment, as shown in Figure 3.10. These fans help create the necessary airflow for the FCs and the heat exchanger within the fuselage. Additionally, the battery provides heating for the FCs, if necessary, e.g. during cold starts, ensuring they quickly reach optimal operating conditions. Auxiliary systems such as air compressors, coolant pumps, and humidity management systems are also activated by the battery to supply the FC with necessary operating media.

Figure 3.10: Fuselage Air Inlet with Integrated

Another advantage of the battery is that it balances the weight of the hydrogen water tank, FCs and the BLI engine at the aft. Using a battery for the power requirement in all mission segments except cruise, also addresses the issue of insufficient air inflow for the FCs during ground operations. Furthermore, the battery provides additional safety as the combination of FCs and battery minimizes the risk of a complete power failure [75].

3.2.4 Propulsion System Specifications

With the operating principle of the drive system established, the exact specifications of the drive system are set out below.

The required energy storage capacity of the battery is based on an interpolation of data from a paper that estimates power total energy requirements for non-propulsive systems. [76] The energy storage capacity was reduced by a conservative approximation of 40% due to the battery not operating during cruise, thereby reducing the onboard battery weight. Furthermore, research suggests that batteries with high gravimetric energy density often come with a trade-off in relatively small volumetric energy density. [77] That is why, although

the gravimetric power density of the battery for 2050 is high, a conservative increase in volumetric power density was assumed. [77]

For the HT-PEMFCs, the specifications are derived from literature review. The volumetric power density of the FC had to be taken from the automotive industry, enabling projections of even higher volumetric power densities than assumed for EcoAir. [78]

To summarize, the Table 3.4 below lists the specifications of the battery and FCs used in the propulsion system.

Table 3.4: HT-PEMFC and Battery Data

Battery		HT- PEMFC	
Total Energy Consumption [76] [MWh]	4	Operating Temperature [71] [°]	160
Volumetric Energy density [77] [kWh/m^3]	230	Volumetric Power density [78] [MW/m^3]	3100
Gravimetric Energy density [79] [kWh/kg]	800	Gravimetric Power density [71] [kW/kg]	16
Total Volume [m^3]	2,2	Total Volume [m^3]	1,7

The mass composition of EcoAir was based on Fly Zero's electric propulsion systems roadmap report. [80] Minor adjustments were made to this mass composition to account for the additional battery and the fact that both the battery and FC stacks were oversized by 20% to achieve the highest operating efficiency and to prolong lifespan [81] [65]. Oversizing the FCs also results in reduced heat production [65], leading to an estimated 10% decrease in thermal management mass. The overall mass composition is illustrated below in Figure 3.11.

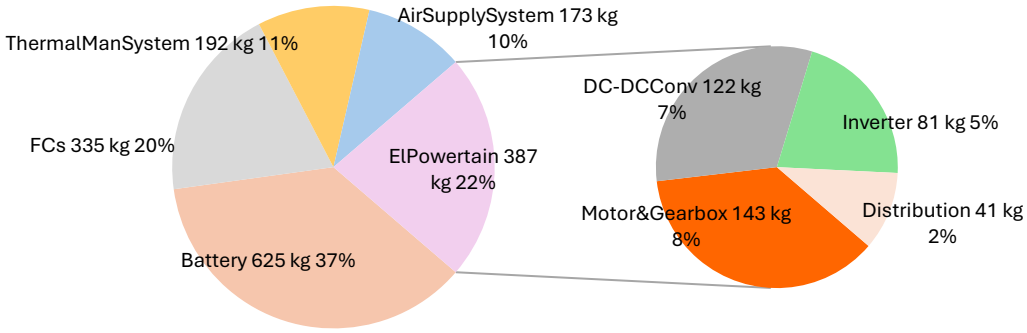

Figure 3.11: Mass Composition of the Electrical Propulsion System

The system's overall efficiency is depicted in Figure 3.12, with each system component's efficiency taken from literature. Only a higher BLI fan efficiency was utilized than previously reported due to the high-power engine and extrapolation for 2050.

Total Efficiency Propeller Engine	**52,5%**
Total Efficiency BLI Engine	**50,7%**
BLI Fan [82]	85%
Propeller [83]	88%
ElPropSystem	**59,7%**
ElPowertrain	**91,8%**
DC-DC Converter [84]	98%
Distribution [60]	99,6%
Inverter [60]	98%
Motor & Gearbox [60]	96%
FC stacks [68]	65%

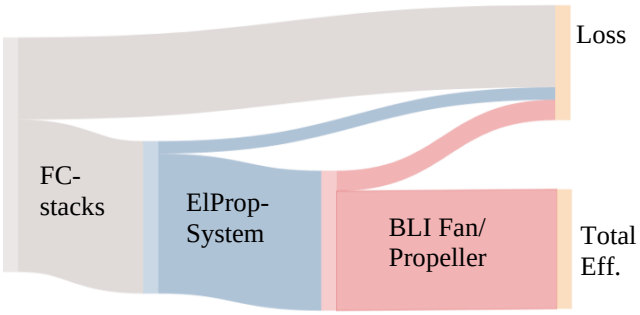

Figure 3.12: Total Electric Propulsion System Efficiency for BLI- and Propeller Engine

3.3 Wing and Empennage

This Chapter provides an overview of the design and integration of the wings and the aircrafts tail in Subchapters 3.3.1 and 3.3.2. As shown in Chapter 3.1.3 EcoAir does not store its fuel in the wings, which results in a unique wing design. Resulting effects and possibilities are discussed in the following.

3.3.1 Wing Design and Integration

The wing design is a result of several different requirements - cruise, ground handling, cost, operational, taxi and terminal requirements. The unique design of EcoAir's dry wings can enhance structural efficiency, aerodynamic performance, and overall aircraft safety. By exploiting the hybrid laminar flow control (HLFC) and use of CFRP innovative design techniques, such as stringers are designed directly to the CFRP, wings are created and optimized for chosen propulsion systems.

Reaching the Flightpath 2050 goals is highly likely obtained by laminar technology. The HLFC, is an active flow control by keeping the flow laminar over wetted surfaces by boundary layer suction during cruise [85] [86]. The integration of CFRP materials in the wing's skin, spars, and ribs, complemented by a honeycomb core, maximizes stiffness and minimizes weight. The leading-edge is a perforated layer made of titanium to suck the boundary layer via pump from the numerous micro holes in the outer sheet through the front chamber to a middle chamber. As seen in Figure 3.13, the main spar at 25% chord length and secondary spar at 60% chord length provide robust support for aerodynamic loads and house the HFLC systems effectively. The 6 redundant suction systems pumps are distributed at the span of the wing.

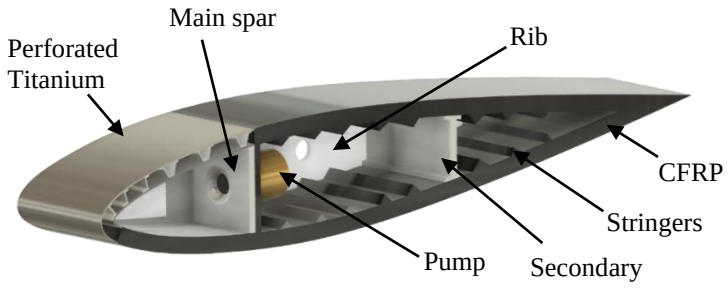

Figure 3.13: HLFC Wing Airfoil Design

The leading-edge chamber of the wing is spacious to fit the anti-icing systems. The wing is integrated into the upper fuselage by securing the main and rear spar to frame of the reinforced fuselage using high strength bolted joints. Using the NACA 63-015 airfoil, with 15% max thickness to chord ratio. Due to no fuel storage and accommodation of extra suction systems and the anti-icing systems this ratio is ideal. The high wing design configuration for this aircraft is a modification to the reference aircraft that can accommodate two engines on each wing. Since no fuel is stored in the wings, thinner and lighter wings are considered. Structural complexity and any fuel-related risks are reduced. The outcome of this is a aircraft with 60.44 m² of wing area and the aspect ratio is slightly risen to 16, in comparison to 12 of the reference aircraft. This results in decrease of lift induces aerodynamic drag because the induced drag coefficient and the aspect ratios are inversely proportional [87]. This improves the aerodynamic performance and efficiency.

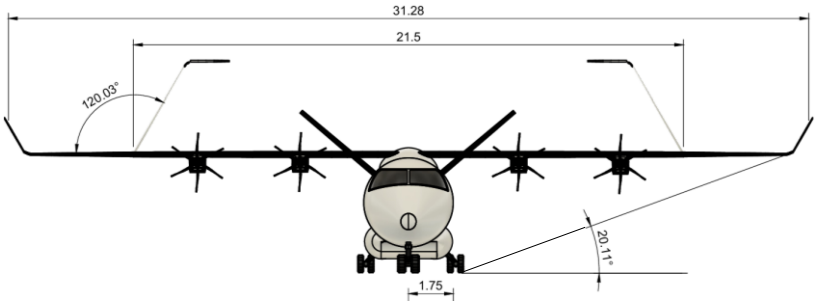

As seen in the Figure 3.14 The higher aspect ratio results is increased wingspan of the aircraft to aprox. 31.28m which is acceptable to maintain the aircraft under Code C of Aerodrome reference code for the airport ground handling.

Figure 3.14: Front View of EcoAir

To be accepted under Code B with a maximum of 24m of wingspan at the Gate, a folding wing design is added, which can be activated during the ground handling (ICAO Annex 14 Vol I, Table 1-1). The folding edge is integrated at the 25% length of the half wingspan, where the folding line is parallel to the airstream [88]. The folding edge is controlled by an actuator. This allows the aircraft to land and be handled in any regional airport reducing the airport handling charges. To further enhance the performance during cruise and take off, and reduce vortex drag, a raked winglet design is considered.

3.3.2 Empennage Design and Integration

Due to the high-wing configuration of the aircraft, a conventional cruciform tail is not feasible. The horizontal tailplane would be positioned in the disturbed airflow from the wings, leading to reduced aerodynamic effectiveness. A T-tail or a V-tail are options that use the airflow above wing and fuselage to ensure manoeuvrability. By combining three control surfaces into two, a V-tail offers the best controllability and stability with the smallest wetted area. Consequently, the needed structural mass and induced drag are reduced comparatively [89].

For EcoAir, a V-tail configuration is chosen. To ensure that this configuration does not impact the flight behaviour negatively, the approach by Purser and Campbell is used [90]. According to these methods, a conventional cruciform empennage is converted into a V-tail without altering the moment coefficients, thus preserving the aircraft's controllability and stability characteristics.

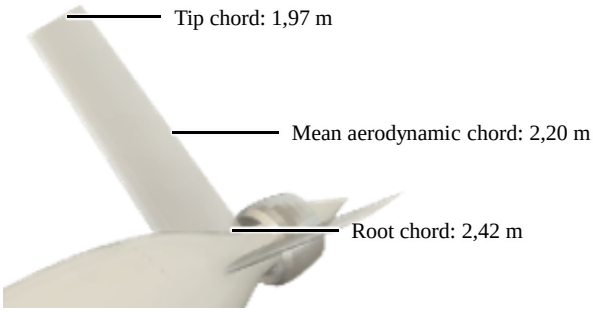

Figure 3.15: V-tail with various chord lengths

Table 3.5: Technical data of the V-tail

Symbol	Parameter	Value
Γ	Dihedral angle	39,9°
S_{v-tail}	Area	28,96 m²
Λ_{v-tail}	Aspect ratio	6
l	Lever	14,22 m

The first step, the design of Horizontal Pail plane (HTP) and Vertical Tail Plane (VTP) is based on methodologies proposed by Raymer [22]. With a static margin of 10,08% of the MAC, static stability is given. To provide lateral stability in standard cruise flight and a critical case of engine failure a positive yawing moment derivative is established. The V-tail's aspect ratio is set slightly higher than that of the HTP as higher loads are expected with combined loads as elevator and rudder [91]. A decrease in wetted area of 36,96% compared to the conventional is established. Characteristic values of the V-tail can be found in Table 3.5.

For EIS in 2050 a 3% reduction in the structural mass of the empennage is anticipated by alleviating the bending moment at the empennage root through Gust Manoeuvre Load Alleviation/Manoeuvre Load Alleviation (GLA/MLA) [92]. A weight reduction of 10% as for the wings cannot be expected. In the case of the wings, this is mainly due to the planned use of CFRP, which is currently common in the empennages [92].

3.4 Flight Performance

This Chapter deals with the operating performance of EcoAir. It is divided into three core evaluations: Mass estimation, aerodynamics and aircraft performance, each of which is crucial for evaluating and optimising EcoAir's capabilities.

3.4.1 Mass Estimation

The mass calculation methods used in this work is based on Raymer and Thorenbeek [22] [41]. Table 3.7 shows the masses of the various components of EcoAir and the equivalentof the reference aircraft, the ATR-72.

Table 3.6: Mass correction coefficients of EcoAir

Component	Correction coefficient
Wing	0.11
Fuselage	0.05
VTP	0.03
Furnishings	0.075
Tank	0,26

A reduced mass can be expected for various components due to improved manufacturing techniques or materials that can be used for EcoAir. These are described in more detail in the corresponding Subchapters of Chapter 3. The respective reduction factor can be found in Table 3.6.

The mass of each subcomponent relative to the maximum take-off mass (MTOM) of EcoAir is shown in Table 3.7. The payload accounts for a share of 29.9 % of the total mass, while the fuselage mass for 16.6 %. In total, payload and fuselage result in approx. 50 % of the total mass.

Table 3.7: Mass Composition of EcoAir and ATR-72

Component	Mass [kg]		Component	Mass [kg]	
	EcoAir	ATR 72		EcoAir	ATR 72
Wing	2567.75	2897.46	Operator Items	1252.00	3110.14
Fuselage	4232.55	2914.95	Systems	1560.20	
HTP	/	175.31	Nacelle BLI	71.83	/
V-tail / VTP	362.52	266.49	Nacelle Prop	383.09	392.42
Nose Gear	100.50	100.50	Fuel Tank	1603.601	0.00
Main Landing Gear	569.50	569.50	Maximum Fuel	912.34	3356.871
Pylon	1068.45	1576.11	Payload	7220.00	7500.00
El-Prop System	866.16	-	Battery	625.00	-
Props	208.38		OEM	16027.90	13082.87
Furnishings/sup	1147.39	1080.00	MTOM	24160.24	23939.74

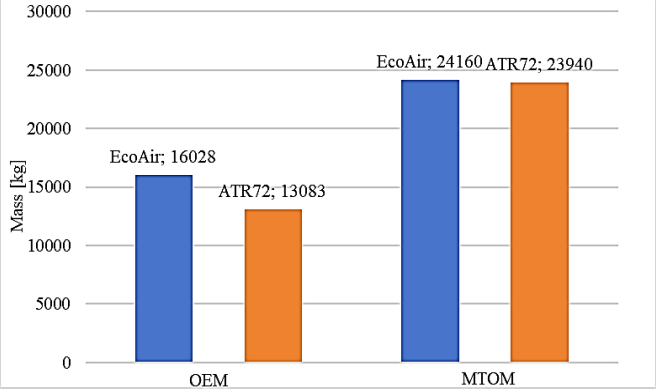

Figure 3.16: Weight Comparison of EcoAir and ATR72

MTOM of the two aircraft differs by approx. 200 kg.

The high percentage of payload indicates EcoAir's high transport capacity and therefore its high commercial value. The masses of every subsystem add up to the Operating Empty Mass (OEM) and the Maximum Take Off Mass (MTOM)displayed in Figure 3.16. The larger OEM results from the increased fuselage diameter and from all those components that are not installed in the reference aircraft. These components are, for instance, the hydrogen tank, the battery, the fuel cells and BLI-engine, as well as the respective related system components, such as cables and electrics. This additional mass is compensated by a significantly lower amount of fuel required for EcoAir. Therefore, the

3.4.2 Aerodynamics

The following Section provides a comparative analysis of aerodynamic performance between the EcoAir and the ATR-72. Figure 3.17 shows the results in terms of total drag coefficient, wherein the positive percentage values show an increase in the drag coefficient of EcoAir with respect to ATR-72, and vice versa for the negative ones. EcoAir exhibits a significant reduction (7%) in the wing's drag coefficient, which can be primarily attributed to increased wing thickness and sweep angle. However, there is an observable increase of 5% because of the V-tail design. The larger and longer fuselage along with the propeller engines causes a notable increase in the total drag coefficient of EcoAir. Nevertheless, there is an overall coefficient decrease by 17% due to the increased aspect ratio of EcoAir. The Figure 3.18 presents a breakdown of the total drag into its individual components. The total drag coefficient exhibits only a slight overall increase, which can be attributed to the offset of the increase in the drag coefficient of the fuselage and the engines by the reduction in the induced drag coefficient and the wing drag coefficient.

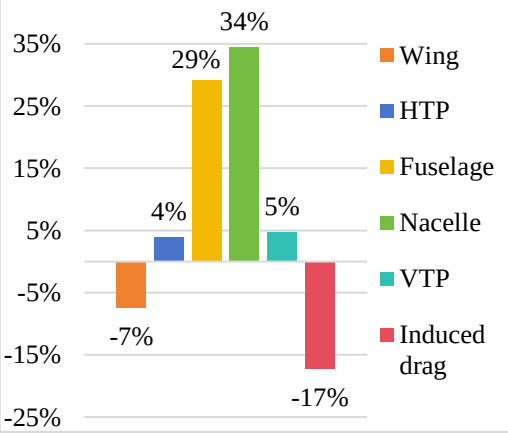

Figure 3.17: Comparison of drag coefficients of different components EcoAir and ATR-72

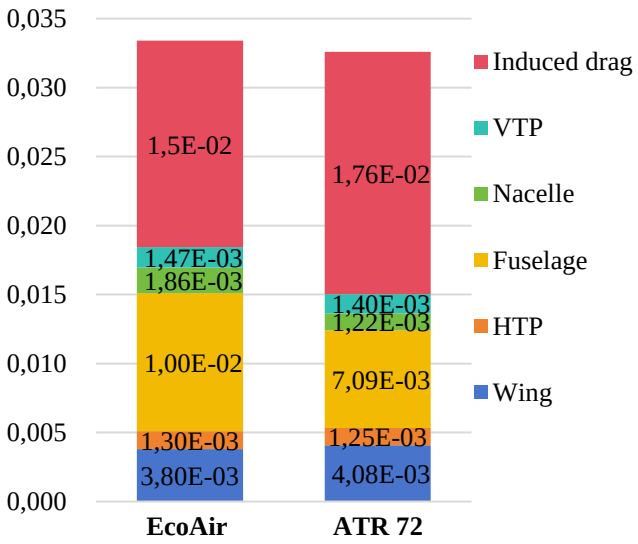

Figure 3.18: Breakdown of the Total Drag into the Individual Components of the EcoAir and ATR72

Figure 3.19 shows the polar drag curves for compressible and incompressible air conditions for the aircraft. An increase in the zero-lift drag coefficient of EcoAir can be observed, as well as an increase of 22% in the lift-to-drag ratio compared to the ATR72. In addition to the 10% increase in L/D, the remaining 12% increase derives from the change in the empennage's lift coefficient and the reduction in induced drag. The increased lift-to-drag ratio improves fuel efficiency, extends range and enhances aerodynamic performance. The wave drag during flight is negligible because of low Mach number of 0,42 at cruise. Therefore, the drag in compressible and incompressible flows does not differ significantly.

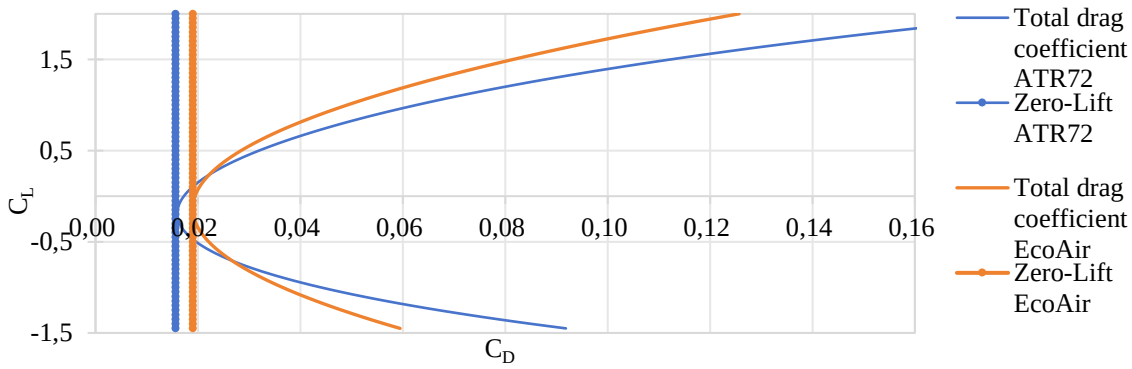

Figure 3.19: Drag Polars for the Compressible and Incompressible Case

The modifications made on the baseline aircraft result in a significantly increase of lift to drag ratios (L/D) as shown in Figure 3.20. A maximum L/D of 20,23 is achieved.

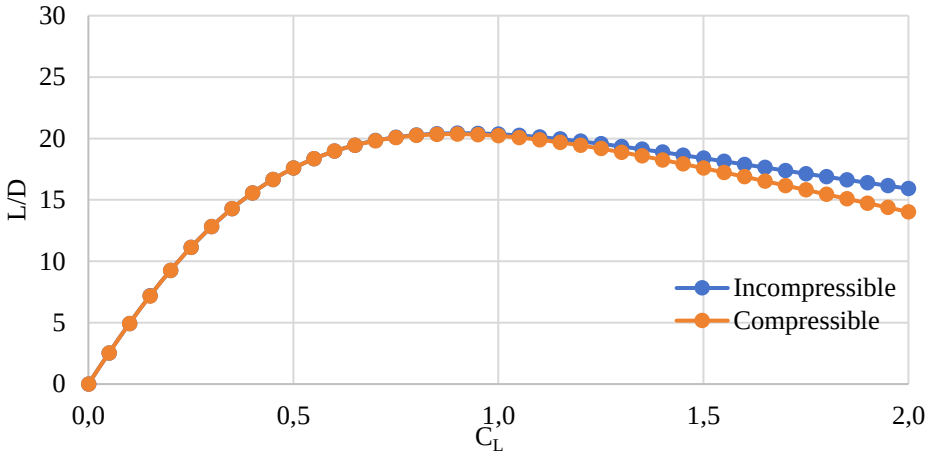

Figure 3.20: The L/D - C_L Trade for the Incompressible and Compressible Case

3.4.3 Aircraft Performance

This Section discusses key points in the flight performance. Figure 3.21 shows the payload range diagram and the use cases for every mission of EcoAir. It can be noted that with the maximum payload of $m_{Pl,max} = 7220\ kg$, a range of $R = 600km$ can be flown; whereas, with a payload decreased to $m_{Pl,min} = 5890\ kg$, the corresponding range increases to $R = 1145\ km$. The marked use cases represent all the routes from the task description with the corresponding payloads, based on the route optimization in Section 2.3. The payload calculation is based on the number of occupied seats by applying the relation $m_{Pl} = PAX \cdot 95\ kg$, as EcoAir only transports passengers and no additional freight. All the flights are arranged around the design point 'x'. If the actual payload is less than the payload value at the design point 'x', the range increases. This relationship is also explained in Chapter 2.3.

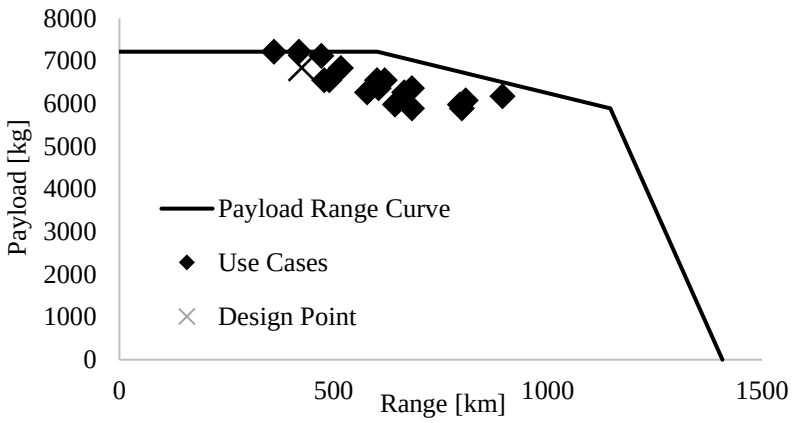

Figure 3.21: Payload- Range Diagram of EcoAir

To study the take-off performance, we consider several parameters, including take-off distance, decision speed, rotation speed and take-off safety speed.

The take of thurst of a single engine of EcoAir is lower compared to a combustion engine of the ATR-72. Due to the configuration consisting of 4 engines and the BLI engine, a take-off field length of 1315 m is sufficient and a climb rate of 1055,64 ft/min is achieved.

Compared to the ATR72, EcoAir achieves shorter landing distances and lower approach speeds, thereby enhancing braking efficiency. In comparison to the ATR-72, EcoAir's approach speed is reduced from 115.9 kts to 107.4 kts, and the landing distance from 1067 m to 915 m. The shorter landing distance reduces the runway length required, allowing for operations at smaller airports and enhancing overall airport accessibility.

During the design process of EcoAir, safety margins and regulatory requirements have been considered, which ensure sufficient runway length beyond the calculated landing distance to accommodate unexpected factors such as gusts, braking inefficiencies, or aircraft system anomalies. Additionally, a tailstrike scenario can be ruled out. Figure 3.22 shows the relationship between the equivalent airspeed and load factor (G-Load). For airspeeds higher than the manoeuvring speed ($v_A = 95.4\ m/s$), the aircraft can withstand full control manouvres without structural damage. For lower air speeds, high lift system is used to achieve the stall speed in landing configuration.

In Figure 3.22 $v_{st} = 57.4\ m/s$ is comparable with the estimated approach speed. The proposed cruise speed of $v_C = 130\ m/s$ is higher than the manoeuvring speed and lower than the never exceed speed ($v_{NE} = 168.9\ m/s$). Differences to both values are sufficiently large to allow for save cruise flight and manoeuvrability.

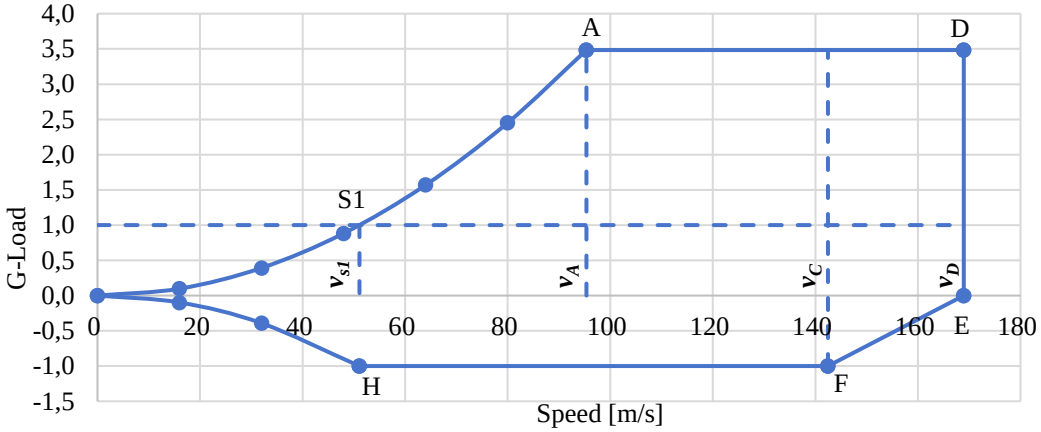

Figure 3.22: V-N-Diagram for Eco Air with stall, descend and cruise speed

The results of the entire aircraft design are summarised in the Table 3.8. It contains the most important technical data of EcoAir, such as geometric dimensions, structural parameters and achievable operating quantaties. The operating requirements specified in the task, such as climb and descent rate, can be met.

Table 3.8: Technical Data of EcoAir

Geometric Dimensions		
Parameter	**Value**	**Unit**
Fuselage		
Fuselage Length	28,45	m
Fuselage Diameter	3,50	m
Wing		
Span	30,86	m
Area	59,52	m²
MAC	1,95	m
Aspect Ratio	16	
Leading Edge Sweep	7,68	°
Empennage		
Diheadral Angle	39,92	°
Area	28,96	m²
Span	13,18	m
MAC	2,20	m
Aspect Ratio	6	
Lever	14,22	m
Landing Gear		
X-Position Nose Landing Gear	2,07	m
X-Position Main Landing Gear	16,81	m
Y-Position Main Landing Gear	0,6	m
Strut Length	1,36	m

Structural Parameters		
Parameter	**Value**	**Unit**
Masses		
MTOM	24160,24	kg
OEM	16037,9	kg
Maximum Fuel Mass	912,341	kg
Maximum Payload	7220	kg
Aerodynamics		
L/D	20,23	
C_L in Cruise Flight	0,5	
Surface Load	340	kg/m²
Operating Quantaties		
Parameter	**Value**	**Unit**
Maximum Range	1340	km
Cruising Speed	0,42	Ma
	471,93	km/h
Cruising Altitude	7620	m
Energy Requirment	12,6	kJ/pax/km
Direct Operating Cost	9,125	$M/year
	0,25	$/PAX/km
Climb rate	1055,64	ft/min
Descent angle	1268,3	ft/min

3.5 Aircraft Systems

This Chapter shows innovative technologies from EcoAir that are not an integral part of the aircraft at the highest manufacturing level, but significantly increase the efficiency of the overall system nevertheless. Aerodynamic perfomance is improved through Hybrid laminar flow control (HLFC) as shown in Chapter 3.3.1. Introducing Hybrid laminar flow control into EcoAir entails introducing 4 main sub-systems, as seem in the Figure 3.23.

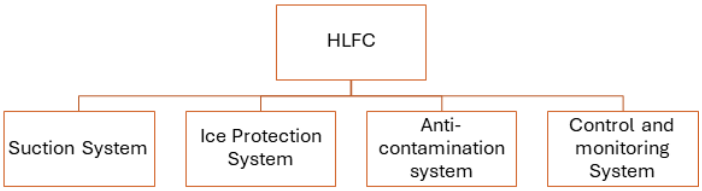

Figure 3.23: HLFC Subsystem architecture

Three electric pumps on each wing that run on electric power suck the air redundantly into the second chamber of the wing where it can be utilized for cooling purposes or just exited out of the wing. Ice accumulation on any part of the aircraft is fatal. Since EcoAir does not rely on bleed air, a new methodology is put into place that can also be compatible with CFRP. The induction anti-icing system is placed under the lower skin of the wing of the leading edge. For this reason, electromagnetic induction heating is an efficient and fast way to heat metallic surfaces from certain distances. Further advantages of this system are- low maintenance cost, safety, precise control, and rapid and efficient heating [93]. This system supports the entire electrification of the aircraft.

Special measures can be taken with the ground handling of the aircraft, since most of the contamination can occur at sea level during the flight [86]. For instance, paper covering, scraper wipers deflectors, etc. Further not only boundary layer conditions but also the mass flow and pressure inside the suction chamber gives the suction system conditions information. The pilot only needs to be warned in case of any malfunction for the fuel insufficiency case for the target destination. For the extra anti-icing system, the temperatures is monitored to avoid ice build ups or overheating of the material.

Important parts include the hydrogen tank, electric motors, power electronics, and fuel cells will all have their health constantly monitored by health monitoring and predictive maintenance system. To anticipate such failures before they happen, real-time data on variables, namely temperature, pressure, voltage, and current, are gathered and examined using machine learning algorithms. By proactively scheduling maintenance tasks, the predictive maintenance system will lower unscheduled downtime and guarantee operational dependability. Comprehensive diagnostics will be possible through integration with the aircraft's overall health management system, prolonging the life of important parts and improving efficiency and safety.

With the rise in commercial flights, a lack of pilots is expected in upcoming years [94]. A Single-Pilot Operation (SPO) cockpit is a new architecture that can be considered to mitigate the load of a single pilot with the contribution of artificial intelligence (AI). This system assists the pilot in navigating through the flight environments using an augmented reality (AR) and verbal communication. However, for a SPO, more automation in the cockpit would exacerbate the paradox of automation by placing additional responsibility for system monitoring on the pilot. However, a co-pilot's traits ought to be included in an assistance system for SPO. Verbal and nonverbal communication are among the functional criteria for such a system [95]. AR has been utilized for many years in aviation to improve navigation in aircraft for nonverbal communication. Increasing the pilot's situation awareness during crucial flight operations like takeoff and landing is the goal of employing AR.

3.6 Technology Readiness of Key Technologies

To assess the maturity level of all key technologies, a Technology Readiness Level (TRL) analysis is conducted. A TRL analysis is a widely used assessment tool in technology development and innovation projects, designed to measure the maturity of a technology or its key components from initial concept to full deployment. [96] The systematically evaluated and ranked TRL of each technology based on literature research suggests that a market entry for EcoAir in 2050 is feasible, as no technology falls below TRL level 4. The rankings are summarised in Table 3.9.

Table 3.9: TRL of Key Technologies

TRL9	Actual System Proven in Operational Environment	Foldable Wingtips [97], Shark skin [98], CFRP [99]
TRL8	System Qualified Through Test and Demonstration	Electrically Motorized Nose Landing Gear [100]
TRL7	System Prototype Demonstration in an Operational Environment	V-Tail [90]
TRL6	System/Subsystem Model or Prototype Demonstration in a Relevant Environment	HT-PEMFC [80], electrically- driven Propulsion System [101], Induction Anti-Icing [102]
TRL5	Component and/or System Validation in Relevant Environment	LH2 Storage and Distribution [53], FC BoP [74]
TRL4	Component and/or System Validation in Laboratory Environment	HLFC [103], BLI Engine [62]
TRL3	Analytical and Experimental Proof-of-Concept	
TRL2	Technology Concept and/or Application Formulated	
TRL1	Basic Principles Observed and Reported	

4 Operations – Optimisation Value Estimation

In the followingChapter, the aircraft concept is evaluated based on the given optimisation goals. The first part discusses fuel masses for all flight phases and estimates block fuel for all connections, from which the used energy per passenger per kilometre is calculated and compared to the reference aircraft. The second part discusses a DOC calculation for the airplane and compares operating cost to the ATR-72 operating on a similar flight plan.

4.1 Flight Paths and Energy

For the given route network, an optimal flight schedule is calculated in Chapter 2.3, which is presented in Table 4.2. The flight frequency indicates the number of round trips per week with the given payload in passengers. For all the flights, a block fuel mass is estimated according to the methods from Raymer. [22]

Table 4.1: Fuel masses [kg] and energy demand [GJ] for each flight phases on one way flight HAM-MUC. Diversion Fuel and Final Reserve is not used, just carried.

Flight phase	Taxi Origin	Contingency	Climb Mission	Cruise Mission	Climb diversion	Cruise diversion	Final Reserve	Additional	Extra Fuel	Taxi Dest.
Fuel Mass	65,77	24,07	221,96	259,34	38,79	77,31	121,27	0	0	35,41
Energy usage	7,89	2,89	26,63	31,11	4,65	9,27	14,55	0	0	4,25

A flight is considered as two independent flights with different optimal block fuel. If an intermediate stop takes place, two individual flights are considered. The trip energy consists of the fuel burned on all flights in one week for each route. The energy is calculated with the used fuel mass and the given caloric mass of hydrogen. The used fuel on each route consists of taxi fuel and trip fuel only. Reserves for diversion, holding and contingency are calculated and loaded but not used. Since two-way flights with a short turnaround are considered, fuel savings due to wind or other natural phenomena are neglected.

Compared to the ATR-72 reference aircraft, EcoAir uses 83% more energy per pax kilometer on route HAM-MUC by considering a base mission of 300 nm with a block fuel of 896 kg for the ATR and for EcoAir (see Table 4.1). It is assumed that only 72% of the fuel is consumed during the flight. The aircraft is fully loaded with 72 (ATR-72) or 69 (EcoAir) passengers.

With the proposed flight plan, the energy consumption of all flights in one week is estimated using Equation (4-1):

$$E_{pax,km} = \frac{20661{,}43\ MJ}{9310\ pax \cdot 211344\ km} = 12{,}7 \frac{kJ}{pax \cdot km} \tag{4-1}$$

Table 4.2: Flight plan indicating Trip distance, total passenger demand, roundtrips per week, used seats per flight, laded block fuel, travelled distance on route per week and used energy per week on all round trips

Route	Distance	Total passenger	Frequency	Payload	Block Fuel	Distance per Week	Energy on route per week
	km	PAX		PAX	kg		MJ
GOT – VBY	361	751	10	76	748,71	7220	1218,67
HAM – RTM	419	228	3	76	776,06	2514	385,29
HAM – ANR	464	177	3	59	757,64	2784	377,96
HAM – GOT	471	1044	14	75	798,27	13188	1874,22
HAM – PRG	490	821	12	69	792,91	11760	1599,43
HAM – LUX	517	356	5	72	812,61	5170	688,31
HAM – MUC	601	1263	18	69	843,92	21636	2619,43
HAM – SVG	643	498	8	63	847,18	10288	1176,05
HAM – BGO	795	559	9	63	915,51	14310	1470,58
GOT – UME	808	634	10	64	924,36	16160	1654,04
HAM – EDI	894	879	14	65	966,44	25032	2455,37
HAM – TRF	478	547	8	69	787,40	7648	1055,71
TRF – TRD	619				852,20	9904	1180,09
HAM – FDH	578	588	9	66	825,68	10404	1273,48
FDH – MRS	665				865,22	11970	1358,85
HAM – SZG	605	534	8	67	840,55	9680	1159,59
SZG – SJJ	683				876,16	10928	1227,94
BRI – SZG	799	431	7	62	914,33	11186	1142,62
SZG – HAM	683				862,39	9562	1055,39
Sum		9310				211344	24973,12

4.2 Direct Operating Costs

The method for Direct Operation Costs (DOC) analysis proposed by Thorbeck [104] is used and adapted to a hydrogen-powered aircraft using the approach by Hoelzen [3]. All costs are presented in $\$_{2019}$. Similar calculations were made for the ATR-72 as a reference aircraft for comparability. Figure 4.1 shows the DOC broken down into its respective categories for EcoAir and ATR-72.

Route-independent costs consist of capital costs (C_cap) and costs of the aircraft's crews (C_crew). The capital costs of EcoAir are higher, due to the higher OEW, which scales directly into it. Nevertheless, since the salary of a pilot can be saved as shown in Chapter 3.5, the crew costs are reduced.

Route-dependent costs, show the additional advantages of EcoAir. The network calculation carried out in the previous Chapter 4.1 is accomplished for both aircraft.

Based on their TLARs, the yearly flight cycles (FC) for an entire fleet were determined to be 7176 for ATR-72 and 7384 for EcoAir. The forced downtime, determined according to the Thorbeck model was applied, resulting in six aircraft required for each fleet. Higher fees (C_fee) must therefore be expected for EcoAir.

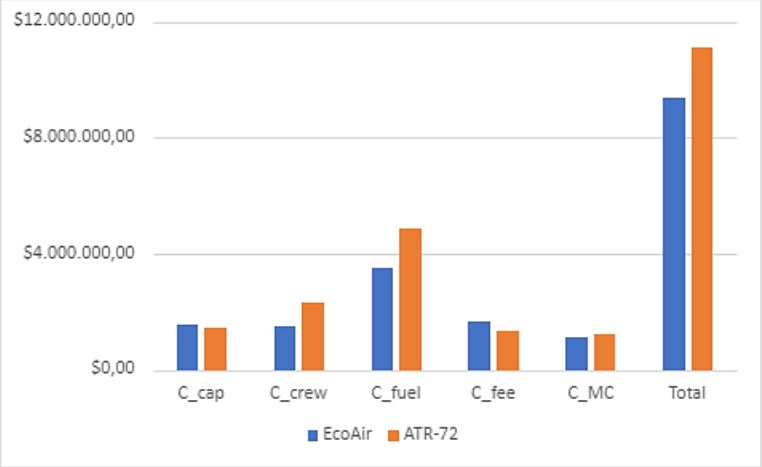

Figure 4.1: DOC for EcoAir (blue) and the ATR-72 (orange)

Figure 4.1 shows that especially the low required trip fuel has a big decreasing influence on the DOC. For hydrogen a price of 0,097 $\$_{2019}$/kWh was assumed. To reasonably compare with the ATR-72 in the year 2050, a SAF price of 0,104 $\$_{2019}$/kWh was used instead of the price of kerosine. Additionally, the required fuel mass for EcoAir is considerably lower. Given these reasons, EcoAir's fuel costs are significantly lower compared to the reference aircraft. Overall, this results in DOC of 11,13M$ for the ATR-72 and 9,36M$ for EcoAir. Therefore, a cost reduction of 15,9% can be expected for EcoAir compared to the ATR-72 in the same scenario of 2050.

5 Conclusion and Recommendations

This paper presented an innovative aircraft design aimed at enhancing operational flexibility and reducing costs. The aircraft features foldable wingtips, allowing it to be classified within a smaller aircraft category. This classification enables the aircraft to access a greater number of airports and benefit from the lower requirements imposed on smaller aircraft.

A motorized nose landing wheel eliminates the need for pushbacks, facilitating autonomous taxiing even at smaller airports where such ground support equipment might be unavailable. These technologies collectively enhance the operational resilience of the aircraft.

The propulsion system is powered by fuel cells (FCs), targeting the aircraft climate neutrality. This system supports unconventional propulsion configurations, including electric motors, reducing both maintenance and manufacturing costs. Further studies indicate that an FC-driven aircraft can substantially decrease the aviation industry's climate impact, with a minimal cost increase of approximately USD 5–10 per passenger (PAX) for commuter and regional aircraft [105]. The design incorporates distributed propeller engines and a Boundary Layer Ingestion (BLI) engine, which together with the Hybrid Laminar Flow Control (HLFC) technology and sharkskin surface technology significantly boost the aircraft's efficiency.

A windowless fuselage design further reduces manufacturing costs and simplifies the production process. Despite the lack of windows, the cabin remains passenger-friendly with a wider layout and OLED screens projecting external views. The aircraft is operated with a single pilot, supported by AI systems to maintain high safety standards while reducing crew costs. Overall, this aircraft concept leverages advanced technologies to deliver a cost-effective, efficient, and environmentally friendly solution for modern air travel.

Although comprehensive analyses, design considerations and calculations were undertaken, recommendations for further investigation are suggested. While the tail shape is designed to ensure uniform air inflow at the nacelle inlet, further investigation is required to address potential boundary layer separation as no numerical calculations were performed at this stage.

The interaction between the wing wake stream and the V-tail should be thoroughly analysed as well, as it may significantly influence performance. Depending on this analysis, a T-tail configuration may be a more optimal choice.

Lastly, it is suggested to explore different reference aircraft with more passenger seats for the same design concept, as this may better align with network optimization goals for ideal passenger capacity and range. However, it is essential to assess the feasibility of these larger designs, as some research suggests that the significantly higher MTOM associated with FC propulsion systems could render larger aircraft designs impractical. [69] [68]

6 References

[1] DLR, "DLR Design Challenge 2024 Tas description," DLR, Braunscheig; Hamburg, 2024.

[2] F. Flemisch and M. Preutenbeck, "Human systems Exploration for Ideation and Innovation in Potentially Disruptive Defense and Securety Systems," in *Disruption, Ideation and Innovation for Defence and Securety*, Cham, Springer, 2022.

[3] J. Hoelzen, D. Silberhorn, Z. Thomas, B. Boris and H.-R. Richard, "Hydrogen-powered aviation and its reliance on green hydrogen infrastructure- Review and research gaps," *International journal of hydrogen energy*, no. 47, pp. 3108-3130, 2021.

[4] K. Dahal, S. Brynolf, C. Xisto, J. Hansson, M. Grahn, T. Grönstedt and M. & Lehtveer, "Techno-economic review of alternative fuels and propulsion systems for the aviation sector," *Renewable and Sustainable Energy Reviews,*, no. 151, 2021.

[5] S. Ulrich, E. Behrend, H. Pohl and N. Rostek, "Hydrogen aircraft and airport safety," *Elsevier BV*, pp. 239-269, 1 Dezember 1997.

[6] S. Tiwari, M. J. Pekris and J. Doherty, "review of liquid hydrogen aircraft and propulsion technologies," *International Journal of Hydrogen Energy*, no. 57, pp. 1174-1196, 2024.

[7] J. Eissele, S. Lafer, C. Mejía Burbano, J. Schließus, T. Wiedmann, J. Mangold and A. Strohmayer, "Hydrogen-powered aviation—design of a hybrid-electric regional aircraft for entry into service in 2040," *Aerospace*, no. 10(3), p. 277, 2023.

[8] C. Sky, "Hydrogen-powered aviation: a fact-based study of hydrogen technology, economics, and climate impact by 2050".

[9] Airbus SE, "Zero-e," [Online]. Available: https://www.airbus.com/en/innovation/energy-transition/hydrogen/zeroe. [Accessed 07 2024].

[10] V. Marciello, M. Di Stasio, M. Ruocco, V. Trifari, F. Nicolosi, M. Meindl and P. Caliandro, "Design exploration for sustainable regional hybrid-electric aircraft: A study based on technology forecasts," *Aerospace*, no. 10(2), p. 165, 2023.

[11] D. Finger, F. Goetten, C. Braun and C. Bil, "ost estimation methods for hybrid-electric general aviation aircraft," *Proceedings of 11th Asia-Pacific International Symposium on Aerospace Technology (APISAT 2019)*, pp. 4-6, December 2019.

[12] H. Gesell, F. Wolters and M. Plohr, "ystem analysis of turbo-electric and hybrid-electric propulsion systems on a regional aircraft," *The Aeronautical Journal*, no. 123(1268), pp. 1602-1617, 2019.

[13] M. Rendón, C. Sánchez, J. Gallo M and A. Anzai, "Aircraft hybrid-electric propulsion: Development trends, challenges and opportunities," *Journal of Control, Automation and Electrical Systems*, no. 32(5), pp. 1244-1268, 2021.

[14] B. Brelje and J. Martins, "Electric, hybrid, and turboelectric fixed-wing aircraft: A review of concepts, models, and design approaches," *Progress in Aerospace Sciences*, no. 104, pp. 1-19, 2019.

[15] N. Thapa, S. Ram, S. Kumar and J. Mehta, "All electric aircraft: A reality on its way," *aterials Today: Proceedings*, no. 43, pp. 175-182, 2021.

[16] A. Gnadt, R. Speth, J. Sabnis and S. Barrett, "Technical and environmental assessment of all- electric 180-passenger commercial aircraft," *Progress in Aerospace Sciences*, no. 105, pp. 1-30, 2019.

[17] Airbus SE, "Airbus E-Fan," 2024. [Online]. Available: https://www.airbus.com/en/innovation/energy-transition/hybrid-and-electric-flight/e-fan-x. [Accessed 07 2024].

[18] B. J. Brelje and J. Martins, "Electric, hybrid, and turboelectric fixed-wing aircraft: A review of concepts, models, and design approaches," *Progress in Aerospace Sciences,* no. 104, pp. 1-19, 2019.

[19] X. Ye, A. Savvarisal, A. Tsourdos, D. Zhang and G. Jason, "Review of hybrid electric powered aircraft, its conceptual design and energy management methodologies," *Chinese Journal of Aeronautics,* no. 34(4), pp. 432-450, 2021.

[20] K. Duffy and R. Jansen, "Partially Turboelectric and Hybrid Electric Aircraft Drive Key Performance Parameters," 8 Juli 2018.

[21] Q. Leer and M. Hoogreef, "Aero-Propulsive and Aero-Structural Design Integration of Turboprop Aircraft with Electric Wingtip-Mounted Propellers," 2022.

[22] D. P. Raymer, Aircraft design: A conceptual approach, American Institute of Aeronautics & Astronautics, 1989.

[23] D. Finger, R. de Vries, R. Vos, C. Braun and C. Bil, "A comparison of hybrid-electric aircraft sizing methods," *In AIAA scitech 2020 forum,* p. 1006, 2020.

[24] E. Cestino, D. Pisu, V. Sapienza, L. Chesta and V. Martilla, "A New Range Equation for Hybrid Aircraft Design," *Aerospace,* no. 10(11), p. 955, 2023.

[25] J. Huete and P. Pilidis, "Parametric study on tank integration for hydrogen civil aviation propulsion," *International Journal of Hydrogen Energy,* no. 46, 2021.

[26] Fly Zero, "FlyZero - cryogenic hydrogen fuel system and storage – roadmap report.," 2022.

[27] T. Young, Performance of the Jet Transport Airplane: Analysis Methods, Flight Operations, and Regulations, John Wiley & Sons, 2017.

[28] P. Okonkwo and H. Smith, "Review of evolving trends in blended wing body aircraft design," *Progress in Aerospace Sciences,* no. 82, pp. 1-23, 2016.

[29] Z. Chen, M. Zhang, C. Yingchum, W. Sang, Z. Tan, D. Li and B. Zhang, "Assessment on critical technologies for conceptual design of blended-wing-body civil aircraft," *Chinese Journal of Aeronautics,* 2019.

[30] R. Wittmann, "Passenger acceptance of BWB configurations," in *Proceedings of the 24th ICAS Congress*, Yokohama, Japan, 2004.

[31] M. Derela, "Development of the D8 transport configuration," *29th AIAA Applied Aerodynamics Conference* , p. 3970, June 2011.

[32] T. Reist and D. Zingg, "High-fidelity aerodynamic shape optimization of a lifting-fuselage concept for regional aircraft," *Journal of Aircraft,* no. 54(3), pp. 1085-1097, 2017.

[33] K. Chen, X. Wang, P. Li and J. Xie, "Modeling and Evaluating Passenger Evacuation and Risk in Blended Wing Body Aircraft Using Continuous Displacement Agents," 2024.

[34] A. Seitz, A. Habermann, F. Peter, F. Troeltsch, A. Castillo Pardo, B. Della Corte, M. Van Sluis, Z. Goraj, M. Kowalski, X. Zhao and T. Grönstedt, "Proof of concept study for fuselage boundary layer ingesting propulsion," *Aerospace,* no. 8(1), 2021.

[35] K. Salem, G. Palaia, P. Bravo-Mosquera and A. Quarta, "A Review of Novel and Non-Conventional Propulsion Integrations for Next-Generation Aircraft," *Designs,* 2024.

[36] L. Menegozzo and E. Benini, "Boundary layer ingestion propulsion: A review on numerical modeling," *Journal of Engineering for Gas Turbines and Power,* p. 142(12), 2020.

[37] Y. Cai, D. Rajaram and D. Mavris, "Simultaneous aircraft sizing and multi-objective optimization considering off-design mission performance during early design," *Aerospace Science and Technology,,* no. 126, 2022.

[38] D. Rajaram, Y. Cai, T. G. Puranik, I. Chakraborty and D. Mavris, "Integrated sizing and multi-objective optimization of aircraft and subsystem architectures in early design," *7th AIAA Aviation Technology, Integration, and Operations Conference* , p. 3067, 2017.

[39] R. Martinez-Val, E. Perez, C. Cuerno and J. Palacin, "ost-range trade-off of intermediate stop operations of long-range transport airplanes," *roceedings of the Institution of Mechanical Engineers, Part G: Journal of Aerospace Engineering*, no. 227(2), 2013.

[40] G. Dantzig and M. Thapa, Linear programming, New York: New York: Springer, 1997.

[41] E. Torenbeek, Advanced Aircraft Design: Conceptual Design, Analysis and Optimization of Subsonic Civil Airplanes, John Wiley & Sons, 2013.

[42] Avions de Transport Regional , "The most fuel efficient regional aircraft," Avions de Transport Regional , [Online]. Available: https://www.atr-aircraft.com/aircraft-services/aircraft-family/atr-72-600/ . [Accessed 18 07 2024].

[43] L. R. Jenkinson, P. Simpkin and D. Rhodes, Civil Jet Aircraft Design, AIAA Education Series. American Institute of Aeronautics and Astronautics (AIAA), 19999.

[44] M. F. Niţă, "Aircraft Design Studies Based on the ATR 72," Hamburg University of applied science, Hamburg, 2008.

[45] P. Jie, Q. Wenfeng, Y. Wentao , Z. Mian and M. Qing'an , "Induction Heating Characteristics of Electroless Ni-Coated," p. 14, 2023.

[46] A. Rodolfo, "Lock-in Thermography for Process Integrated Non-Destructive Evaluation of Carbon Fibre Reinforced Aircraft Stuctures," in *10th International Conference on Quantitative InfraRed Thermography*, Québec, 2010.

[47] S. Kuntzagk, *Aeroshark –Drag Reduction Using Riblet Film on Commercial Aircraft.*

[48] B. Orson, "Sustainable Cabin Design-New Approaches in Sustainable Aircraft Interior Design.".

[49] S. A. Resetar, J. Curt Rogers and R. W. Hess, Advanced airframe structural materials, Santa Monica: RAND, 1961.

[50] D. Verstraete, "The Potential of Liquid Hydrogen," Cranfield, 2009.

[51] P. Rompokos, R. Adrew, N. Devaiah, I. Askin T., S. Capucine, G. Tomas and A. Hamidreza, "Synergistic Technology Combinations for Fotore Commercial Aircraft Using Liquid Hydrogen," *Journal of Engineering for Gas Turbines and Power*, no. 143, July 2021.

[52] S. K. Mital, J. Z. Gyekenyesi, S. M. Arnold, R. M. Sullivan, J. M. Manderscheid and P. L. Murthy, "Review of current state of the art and key design issues with potential soultions for liquid hydrogen cryogenic storage tank structures for aircraft applications," 2006.

[53] D. Silberhorn, G. Atanasov, J.-N. Walther and T. Zill, "Assessment of hydrogen fuel tank integration at aircraft level," Darmstadt, 2019.

[54] G. D. Brewer, Hydrogen aircraft technology, New York: Routledge, 1991.

[55] FlyZero, "Realising zero-carbon emission flight," 09 September 2021. [Online]. Available: https://www.ati.org.uk/wp-content/uploads/2021/09/FZ_0_6.1-Primary-Energy-Source-Comparison-and-Selection-FINAL-230921.pdf. [Accessed 16 July 2024].

[56] J. Mangold, D. Silberhorn, N. Meabs, N. Dzikus, J. Hoelzen, T. Zill and A. Strohmayer, "Refueling of LH2 Aircraft—Assessment of Turnaround Procedures and Aircraft Design Implication," *Energies*, no. 15, 2022.

[57] U. Schmidtchen, E. Behrend, H.-W. Pohl and N. Rostek, "Hydrogen aircraft and airport safety," *Renewable and sustainable energy reviews,* vol. 1, pp. 239-269, 1997.

[58] N. Moirou, D. Sanders and P. Laskaridis, "Advancements and Prospects of Boundary Layer Ingestion Propulsion," *Progress in Aerospace Sciences,* vol. 138, 2023.

[59] H. D. Kim, A. T. Perry and P. J. Ansell, "A Review of Distributed Electric Propulsion Concepts for Air Vehicle Technology," *2018 AIAA/IEEE Electric Aircraft Technologies Symposium (EATS),* pp. 1-21, 2018.

[60] J. Welstead and J. Felder, "Conceptual Design of a Single-Aisle Turboelectric Commercial Transport with Fuselage Boundary Layer Ingestion," 2016.

[61] A. Yildirim, Robust Methods for Aeropropulsive Design Optimization, Doctoral dissertation.

[62] A. Seitz, F. Peter, J. Bijewitz, A. L. Habermann, Z. Goraj, M. Kowalski, A. C. Pardo, C. A. Hall, F. Meller, R. S. Merkler, O. Petit, S. Samuelsson, B. D. Corte and e. al., "Concept validation study for fuselage wake-filling propulsion integration," *31st Congress of the International Council of the Aeronautical Sciences,* 2018.

[63] H.-J. Steiner, P. Vratny, C. Gologan, K. Wieczorek, A. Isikveren and M. Hornung, "Optimum number of engines for transport aircraft employing electrically powered distributed propulsion," *CEAS Aeronautical Journal,* vol. 5, pp. 157-170, 2014.

[64] D. Keller, "Towards higher aerodynamic efficiency of propeller-driven aircraft with distributed propulsion," *CEAS Aeronautical Journal,* vol. 12, 2021.

[65] D. Debney and et al., "Zero-Carbon Emission Aircraft Concepts," *Fly Zero Aerospace Technology Institute,* Vols. FZO-AIN-REP-0007, 2022.

[66] European Union Aviation Safety Agency (EASA), "Type certificate data sheet for engine PW100 series engines," *European Union Aviation Safety Agency,* vol. No. IM.E.041, 2023.

[67] D. Diamantidou, M. Hosain and K. Kyprianidis, "Recent Advances in Boundary Layer Ingestion Technology of Evolving Powertrain Systems," *Sustainability,* vol. 14, 2022.

[68] J. Mukhopadhaya, "Performance analysis of fuel cell retrofit aircraft," *International Council On Clean Transportation,* 2023.

[69] A. Scholz, J. Michelmann and M. Hornung, "Fuel Cell Hybrid-Electric Aircraft: Design, Operational, and Environmental Impact," 2022.

[70] M. Massaro, R. Biga, A. Kolisnichenko, P. Marocco, A. Montverde and M. Santarelli, "Potential and technical challenges of on-board hydrogen storage technologies coupled with fuel cell systems for aircraft electrification," *Journal of Power Sources,* vol. 555, 2023.

[71] W. Bhatti and et al., "Fuel Cells- Roadmap Report," *Fly Zero Aerospace Technology Institute,* Vols. FZO-PPN-COM-0033, 2022.

[72] M. Schröder, F. Becker and C. Gentner, "Optimal design of proton exchange membrane fuel cell systems for regional aircraft," *Energy Conversion and Management,* 2024.

[73] E. Reshotko, "Drag Reduction by Cooling in Hydrogen-Fueled Aircraft," *Journal of Aircraft,* vol. 16, no. 9, pp. 584-590, 1979.

[74] G. Renouard Vallet, M. Saballus, G. Schmithals, J. Schirmer, J. Kallo and K. A. Friedrich, "Improving the environmental impact of civil aircraft by fuel cell technology: Concepts and technological progress," *Energy & Environmental Science,* vol. 3, pp. 1458--1468, 2010.

[75] C. Yang, Z. Lu, W. Wang, Y. Chen and B. Xu, "Energy management of hybrid electric propulsion system: Recent progress and a flying car perspective under three-dimensional transportation networks," *Green Energy and Intelligent Transportation,* vol. 2, 2022.

[76] Aerospace Technology Institute (ATI), "Electrical Power Systems," *INSIGHT*, vol. 7, 2018.

[77] P. Singh, "Trends in the Gravimetric and Volumetric Energy Densities of Lithium-Ion Batteries Over the Past Decade," 2023.

[78] Toyota Motor Corporation, "All you need to know about the Mirai," 2014. [Online]. Available: https://www.toyota-europe.com/news/2014/mirai-hydrogen-car. [Accessed 11 07 2024].

[79] M. Gill, "Waypoint 2050," *Air Transportation Action Group*, 2020.

[80] K. Mehta and e. al., "Electrical Propulsion Systems - Roadmap Report," *Fly Zero Aerospace Technology Institute*, Vols. FZO-PPN-COM-0033, 2022.

[81] T. Kadyk, C. Winnefeld, R. Hanke-Rauschenbach and U. Krewer, "Analysis and Design of Fuel Cell Systems for Aviation," *Energies*, vol. 11, no. 375, 2018.

[82] P. F. Pelz, S. Saul and J. Brötz, "Efficiency Scaling: Influence of Reynolds and Mach Numbers on Fan Performance," *Journal of Turbomachinery*, vol. 144, no. 6, 2022.

[83] R. Thijssen, P. Proesmans and R. Vos, "Propeller Aircraft Design Optimization for Climate Impact Reduction," *ICAS PROCEEDINGS 33th Congress of the International Council of the Aeronautical Sciences (ICAS)*, 2022.

[84] M. Nymand and M. Andersen, "High-Efficiency Isolated Boost DC-DC Converter for High-Power Low-Voltage Fuel-Cell Applications," *Industrial Electronics*, vol. 57, pp. 505 - 514, 2010.

[85] M. Horn, A. Seitz and M. Schneider, "Cost-effective HLFC design concept for transport aircraft," Stuttgart, 2019.

[86] K. Krishnan, O. Bertram and O. Seibel, *Review of Hybrid Laminar Flow Control Systems*, Braunschweig.

[87] J. D. Anderson, Fundamentals of aerodynamics, New York: McGraw-Hill, 1991.

[88] B. S. Kidane and E. Troiani, Static Aeroelastic Beam Model Development for Folding Winglet Design.

[89] M. U. Khan, M. D. Khan, N. A. Din, M. Z. Babar and M. F. Hussain, "Aerodynamic comparison of unconventional aircraft tail setup," IEEE, 2019.

[90] P. E. Purser and J. P. Campbell, "Experimental verification of a simplified vee-tail theory and analysis of available data on complete models with vee tails," Langley memorial aeronautical laboratory, 1945.

[91] S. Gudmundsson, Gnereal aviation aircraft design: Applied methods and procedures, Waltham, MA: Elsevier, 2014.

[92] C. Xisto and A. Lundbladh, "Design and performance of liquid hydrogen fuelled aircraft for year 2050 EIS," in *33rd congress of the international council of aeronautical sciences*, Stockholm, Sweden, 2022.

[93] I. Villar, . U. Iruretagoyena, A. Cardenas and F. Redondo, "Induction Application to Aircraft Ice Protection System," 2019.

[94] N. Minaskan, C. Alban-Dromoy, A. Pagani, J.-M. Andre and D. Stricker, *Human intelligent machine teaming in single pilot operation: A case study.*

[95] M. Cummings, A. Stimpson and M. Clamann, *Functional Requirements for Onboard Intelligent Automation in Single Pilot Operations.*

[96] C. G. Manning, "Technology Readiness Levels," NASA, 2023. [Online]. Available: https://www.nasa.gov/directorates/somd/space-communications-navigation-program/technology-readiness-levels/. [Accessed 20 07 2024].

[97] Boeing, [Online]. Available: https://www.boeing.com/commercial/777x#overview. [Accessed 24 July 2024].

[98] Lufthansa Technik, "Lufthansa Technik," Lufthansa Group, November 2019. [Online]. Available: https://www.lufthansa-technik.com/en/aeroshark. [Accessed 21 July 2024].

[99] A350, "Airbus Aircraft," Airbus, 2024. [Online]. Available: https://aircraft.airbus.com/en/aircraft/a350-clean-sheet-clean-start/a350-less-weight-less-fuel-more-sustainable#airframe. [Accessed 21 July 2024].

[100] B. Sarlioglu and C. Morris, "More Electric Aircraft: Review, Challenges, and Opportunities for Commercial Transport Aircraft," *IEEE Transactions on Transportation Electrification,* no. Vol 1 No 1, June 2015.

[101] A. Varyukhin, V. S. Zakharchenko, A. V. Vlasov, M. Gordin and M. A. Ovdienko, "Roadmap for the Technological Development of Hybrid Electric and Full-Electric Propulsion Systems of Aircrafts," *International Conference on Electrotechnical Complexes and Systems (ICOECS)*, 2019.

[102] Clean Aviation, "Clean Aviation," Horizon Europe European Union Funding for Research & Innovation, [Online]. Available: https://clean-aviation.eu/media/results-stories/breaking-the-ice-with-clean-sky-innovations. [Accessed July21 2024].

[103] A. Pohya, *Selected current challenges in the development of hybrif laminar flow control on transport aircraft.*, Hamburg.

[104] J. Thorbeck, “DOC-Assessment Method,” Linköping, Sweden, 2013.

[105] O. Fakhreddine, Y. Gharbia, J. Farrokhi Derakhshandeh and A. Amer, "Challenges and Solutions of Hydrogen Fuel Cells in Transportation Systems: A Review and Prospects," *World Electric Vehicle Journal*, vol. 14, 2023.

[106] N. Detsios, S. Theodoraki, L. Maragoudaki, K. Atsonios, P. Grammelis and N. Orfanoudakis, "Recent advances on alternative aviation fuels/pathways: A critical review," *Energies*, no. 16(4), p. 1904, 2023.

[107] P. Giannakakis, P. C and T. A, "Turbo-electric propulsive fuselage aircraft BLI Benefits: A design space exploration using an analytical method," *The Aeronautical Journal*, pp. 1523-1544, 2020.